Babeș-Bolyai University
Faculty of Physics
– Doctoral School of Physics –

Doctoral thesis summary

Fluorophore-Loaded Protein Nanoparticles as Theranostic Agents for the Interventional Imaging and Multimodal Therapy of Ovarian Cancer

Raluca Borlan

Scientific Advisor
Prof. Dr. Simion Aștilean

Cluj-Napoca
2021

Introduction

Cancer is the second leading cause of death around the globe, being responsible for more than 25000 new cases every day. Despite recent years' advances in cancer research, only a few new techniques have significantly changed the course of this disease. The emergence of nanotechnology for medicine heralds a new paradigm in the fight against cancer by providing real-time feedback to surgical oncologists during surgery, contrary to the classical pre-operative imaging techniques which cannot be implemented in the operating theatre. Surgery is usually the first and the most effective treatment option for cancer in combination with perioperative systemic treatment in selected cases, however relapse of disease is a clinical reality. If the pathological report describes positive resection margins, a second intervention might represent a challenge given the patients postoperative status, which could not tolerate a second large intervention.

In this clinical context, in recent years, state of the art near-infrared (NIR) fluorophores encapsulated in nanoparticles have gained popularity as fluorescent probes and contrast agents for the interventional imaging of cancer. The implementation of fluorophores with emission in the NIR region of the spectrum (700 nm -1200 nm), also known as the biological spectral window, provides clear advantages for imaging of tumours during cancer surgery due to the low autofluorescence (generating background-free imaging) and deep tissue penetration of NIR light. Although organic fluorophores remain the cornerstone of NIR contrast agents for fluorescence imaging, due to their low photostability, poor quantum yield, tendency to aggregate in physiological environment, short circulation time and hydrophobic properties, the research community is seeking alternatives to using free form fluorophores in systemic administration. Thus, to enhance and maintain their utility for a prolonged period of time during tumour therapy and molecular imaging, an evolving technique is the encapsulation of the NIR therapeutic and fluorescent agents within targeting nanocarriers, that will not cause a toxic effect to living tissue. Fluorophore-encapsulated nanoparticles with diameters in the optimal size range circulate in the blood for an extended period of time. And thanks to their high loading capacity and protective properties they overcome the poor photostability of free NIR therapeutic and fluorescent agents. Another main advantage of implementing NIR fluorescent nanoparticles vs. free fluorophores as therapeutic and fluorescent agents is their preferential accumulation at tumour site. This phenomenon is achieved through passive tumour targeting done by the enhanced permeability and retention effect (EPR effect), or through active targeting of specific cancer markers by decorating the nanoparticles with appropriate antibodies or other ligands. Thus, novel advancements in the fabrication and implementation of tailored nanoparticles could readily translate to clinical settings for the visualization and resection of tumour, and even assistance in the treatment of cancer itself.

Valued benefits can be provided by encapsulating photosensitive and thermal agents within nanocarriers, due to their upgraded physical, photochemical and biological properties, in comparison to the free molecules' therapeutic performances. Thus, nanoparticles loaded with NIR molecules that reveal photothermal and photodynamic features simultaneously gained a lot of attention as dual therapeutic agents for the

photodynamic (PDT) and photothermal (PTT) therapy of cancer. Moreover, phototherapeutic nano-sized agents can be implemented as adjuvants in surgery to cure this disease, or even to act as a vaccine able to detect and kill cancer cells, by activating a systemic antitumour immune response.

Hereinafter, my doctoral thesis is made up of two main parts: the **First Part**, *Nanobiophotonics for medicine: State of the art and a brief literature review* comprising Chapters 1 and 2, and the **Second Part**, *Original contributions*, made up of Chapters 3 to 6.

To meet current needs, **Chapter 1**, *Cancer-related concerns and state of the art nanobiophotonics approaches for treatment and imaging*, summarises the contemporary challenges and cutting-edge solutions to diagnose and treat cancer, with an emphasis on NIR fluorescence imaging, PTT and PDT.

Chapter 2, *Brief review on next generation of fluorophore-loaded protein-based nanoparticles for interventional NIR fluorescence imaging of cancer*, covers the latest advancements in interventional imaging techniques in literature and outlines the importance of using NIR contrast agents. In addition, chapter 2 includes an up-to-date overview on the biocompatibility, specific targeting and versatility offered by NIR fluorophore-loaded protein-based nanoparticles as next generation of anti-cancer agents and a summarization of the newest and most relevant clinical trials in real-time interventional NIR fluorescence imaging of cancer using state of the art NIR fluorescent agents.

In **Chapter 3**, *Design and characterisation of fluorophore-loaded albumin nanoparticles*, is focused on the design, fabrication, and characterization of fluorophores encapsulated within albumin-based nanoparticles. Thus, four fluorescent molecules have been selected as follows: two fluorophores approved by the Food and Drug Administration (FDA) (Fluorescein Isothiocyanate – FITC – and Indocyanine Green – ICG) and two newly synthesised phthalocyanine dyes, with optical responses from the visible to the NIR region of the electromagnetic spectrum. The albumin nanoparticles were fabricated following a two-step protocol, desolvation using an organic solvent, namely ethanol, and stabilization by chemical cross-linking with glutaraldehyde. Afterwards, the optical and morphological characterisation of all four types of nanoparticles is presented.

Chapter 4, *Targeting and cellular uptake of newly fabricated fluorophore-loaded protein-based nanoparticles by ovarian cancer cells*, focuses on the biofunctionalization of the afresh designed nanoparticles with folic acid molecules and anti-folate receptor alpha antibody proteins, in order to bind specifically to the folate receptor alpha protein overexpressed at the surface of most ovarian cancer cells. In solution characterization of the targeting albumin nanoparticles was discussed, together with time-stability studies. In addition, the biocompatibility and cellular uptake of the newly synthesized nanoparticles were investigated on three different ovarian cancer cell lines. Thus, MTT viability assays were carried out to attest the non-cytotoxic character of the nanoparticles, while their improved targeting capabilities and preferred cellular internalization mechanisms were studied by implementing *in vitro* fluorescence and transmission electron microscopy (TEM) imaging.

Chapter 5, *Assessment and validation of the phototherapeutic activity of fluorophore-loaded protein-based nanoparticles,* pinpoints the biomedical applicability of the

phototherapeutic nanoparticles, by monitoring their dual phototherapeutic character in solution, *in vitro*, *in vivo* and *ex vivo.* The in solution investigations determined the efficiency of the fluorophore-loaded albumin nanoparticles to convert light-to-heat, and their quantum yield to generate the cytotoxic singlet oxygen. The multimodal phototherapeutic effect of our albumin nanoparticles was studied *in vitro* by using MTT, fluorescence imaging and flow cytometry investigations to determine the cell viability after exposure to light. To attest the performance of the fluorophore-loaded albumin nanoparticles in a living model, *in vivo* and *ex vivo* investigations were carried out on ovarian cancer tumour bearing mice. Post nanoparticles administration, the mice were exposed to a 660 nm LED lamp to trigger the photodynamic properties of the nanoparticles and monitor in real-time the photothermal treatment process. In addition, *ex vivo* histopathological analysis of tumour xenografts was performed.

The last chapter, **Chapter 6**, *Revealing the potential of fluorophore-loaded protein-based nanoparticles for the interventional real-time imaging of ovarian cancer*, is the stepping stone in validating our fluorophore-loaded albumin nanoparticles as targeting contrast agents for the NIR fluorescence-guided cancer surgery. Hereinafter, we employed three optical microscopy techniques (conventional fluorescence microscopy, fluorescence lifetime imaging (FLIM) and rescan confocal microscopy) to study *in vitro* our afresh synthesized fluorophore-loaded nanoparticles. The increased rate of targeting nanoparticles within ovarian cancer cells was proven via *in vitro* fluorescence imaging, while FLIM investigations confirmed the different internalization pathway of targeting nanoparticles, as to non-targeting ones. Confocal NIR fluorescence imaging was employed to prove the potential of NIR fluorophore-loaded nanoparticles to be translate in the near future as contrast agents for the the *in situ* NIR image-guided detection and resection of cancerous tissue.

In a nutshell, the first part of my doctoral thesis brings to light the recent advancements towards the clinical translation of NIR fluorophore-loaded protein-based nanoparticles as fluorescent contrast agents for cancer; while the second part provides an insight into the validation of the newly developed nanoparticles as multimodal phototheranostic agents able to combine synergistically fluorescence imaging and dual phototherapeutic features to combat ovarian cancer. The final part of my thesis summary, entitled **Final conclusions and perspectives**, brings up conclusive evidence that our tailored nanoparticles, with optical properties from the visible to the NIR region of the spectrum, have great potential as therapeutic and fluorescence imaging nanoagents for the surgery of ovarian cancer in the never-ending fight against this disease; some perspectives are presented at the end of this chapter.

“I am among those who think that science has great beauty.”

Marie Curie

Key words: fluorescence, nanoparticles, fluorescent contrast agents, ovarian cancer, photodynamic therapy, photothermal therapy, near-infrared imaging.

Table of Contents

Part I. Nanobiophotonics for medicine: State of the art and a brief literature review 1

Chapter 1. Cancer-related concerns and state of the art nanobiophotonics approaches for treatment and imaging 1

1.1 Current concerns 1

1.2 Photoactive agents for cancer imaging and therapy 1

Chapter *2*. Brief review on next generation of fluorophore-loaded protein-based nanoparticles for interventional NIR fluorescence imaging of cancer 4

2.1 Why is NIR so desired? 4

2.2 Employment of nanotechnology in biomedical applications 4

2.3 Protein-based nanoparticles 5

Part II. Original contributions 6

Chapter 3. Design and characterisation of fluorophore-loaded albumin nanoparticles ... 6

3.1 Experimental design outline and fluorophore-loaded albumin nanoparticles fabrication .. 6

3.2 Spectroscopic characterization 8

3.3 Physical properties and particle yield 10

3.4 Albumin-dye interplay and loading efficiency 12

Chapter 4. Targeting and cellular uptake of newly fabricated fluorophore-loaded protein-based nanoparticles by ovarian cancer cells 13

4.1 Biofunctionalization of the nanoparticles with ovarian cancer-specific ligands 13

4.2 Characterization of active targeting fluorophore-loaded nanoparticles in solution 13

4.3 Cell viability assay 15

4.4 Cellular uptake by fluorescence microscopy 15

4.5 Cellular uptake by TEM 16

Chapter 5. Assessment and validation of the phototherapeutic activity of fluorophore-loaded protein-based ……nanoparticles 18

5.1 Phototherapeutic effects: in solution assay 18

5.2 Phototherapeutic effects: *in vitro* assay 20

5.3 Phototherapeutic effects: Translation to murine models 23

Chapter 6. Revealing the potential of fluorophore-loaded protein-based nanoparticles for the interventional real-time imaging of ovarian cancer 24
6.1 Visible fluorescence imaging: FITC-loaded albumin nanoparticles 24
6.2 Deep red fluorescence imaging: phthaloNO_2-loaded albumin nanoparticles 24
FLIM analysis 26
6.3 NIR fluorescence imaging: ICG-loaded albumin nanoparticles 28
Final conclusions and perspectives 30
References 34
Dissemination 36

Part I. Nanobiophotonics for medicine: State of the art and a brief literature review

Chapter 1. Cancer-related concerns and state of the art nanobiophotonics approaches for treatment and imaging

1.1 Current concerns

Worldwide, cancer is the second leading cause of death, reaching by 2018 the appalling total of 9.6 million deaths [1], while by 2017, the global population diagnosed with cancer reached 1.3% [2]. Among females, ovarian cancer ranks fifth in most common cancers and is the sixth leading cause of cancer death[3], with over 200.000 deaths in 2020. There are three cell types that stand at the origin of most benign and malignant ovarian tumours: epithelial cells, stromal cells and germ cells. Nearly all malignant ovarian tumours are epithelial cells in origin. Folate receptor alpha (FRα) is a surface protein overexpressed in several epithelial malignancies, and in 80% of epithelial ovarian cancers, while its expression in healthy tissue is largely absent. Thus, its expression in tumours suggest that this antigen might have potential as a diagnostic marker.

Although prodigious amounts of research were conducted over the past century to improve the current treatment options of cancer, no genuine changes were made to the *sine qua non* of treatment for tumours, namely surgery [4]. Wistfully, none of the different imaging modalities used for tumour detection and surgical planning in a preoperative setting e.g., computed tomography, positron emission tomography, single-photon emission computed tomography, planar scintigraphy, magnetic resonance imaging, can be translated in the operating theatre due to poor tissue manipulation and mismatched patient position [5–7]. Moreover, although the high-resolution eyes (50 µm [8]) and hands of the surgeon can easily distinguish anatomical structures, during resection it is challenging to differentiate between healthy tissue and malignant lesions ending in the undesired removal of healthy tissue or an incomplete resection. After surgery, it can take up to 7 days for the pathology report to be sent to the doctor and in the unfortunate event of positive margins, a reintervention is not recommended, the patient being in recovery [4,8]. Thus, a new strategy to cure and detect cancer and concomitantly give a real-time feedback during surgery is needed in order to suppress this disease [6].

1.2 Photoactive agents for cancer imaging and therapy

A novel approach in curing and detecting malignant tissue is the multidisciplinary field of biophotonics. Biophotonics refers to the interaction of light with cells and biological tissue

and is composed of different branches of science such as photonics, optics, biotechnology and nanotechnology. Being less damaging than gene therapy, chemotherapy and other classical cancer treatments, in recent years biophotonics appealed to medical oncologists as an emerging technique for the treatment, and even imaging of cancer, enabling early diagnosis. Moreover, plentiful basic spectroscopic techniques can be readily applied as biophotonic tools, allowing us to get a better perspective on the current and even future treatment plans and diagnostic approaches.

Over the past few years, phototherapy and fluorescence imaging have been forging ahead in clinical settings as non-invasive therapeutic and diagnosis techniques for outpatient cancer care and real-time feedback during tumour resection [9,10]. These light-based approaches hinge on the properties of photoactive molecules to absorb light and decay to the ground state by i) heat generation, ii) intersystem crossing and iii) fluorescence emission. Each energy dissipation pathway can be attributed to a specific treatment and diagnosis technique, respectively PTT, PDT and fluorescence imaging [11], as illustrated in **scheme 1.1**.

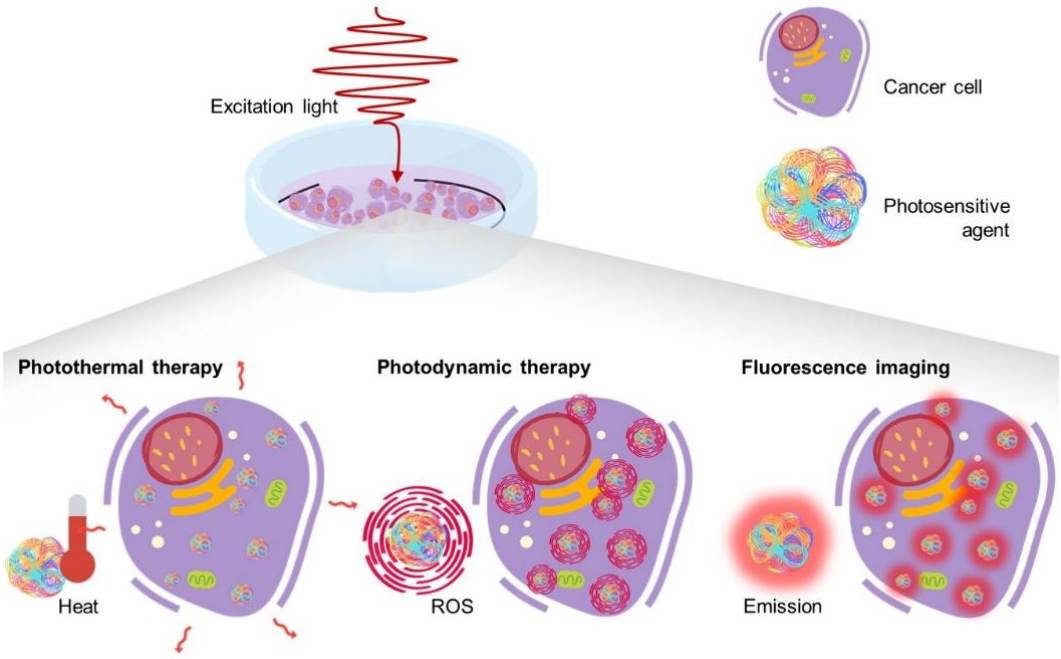

Scheme 1.1. Schematic representation of the synergistic photothermal, photodynamic and fluorescence capabilities of photoactive agents.

PDT is an upcoming treatment alternative to the *gold standard* methods [12], used not only to cure early stage cancer, but also as a viable choice for late-stage cancer in addition to surgery [13]. In the presence of molecular oxygen (O_2), the photochemical reactions between the photosensitizer agents and light [14] lead to the formation of highly cytotoxic

reactive oxygen species (ROS), predominantly singlet oxygen ($^1O_2$), and toxic radicals[15–17]. It is important to note that the FDA already approved PDT as a medical procedure for different types and stages of cancer, using generally phthalocyanine, porphyrin, chlorin or bacteriochlorin molecules as photosensitizing agents [9,16].

Another cancer therapy that has potential to be translated to clinical use is PTT. Aside from light, this therapy involves thermal agents that absorb and then convert light into heat, when the electromagnetic radiation has a suiting wavelength. In biomedical applications, these thermal treatments rely on the local heating of the tissue or desired organ, in a very specific time frame. This kind of treatment is very efficient in theory, but, in real life, it presents significant drawbacks when using free thermal agents due to their lack of distinction between healthy and cancerous tissue[18,19].

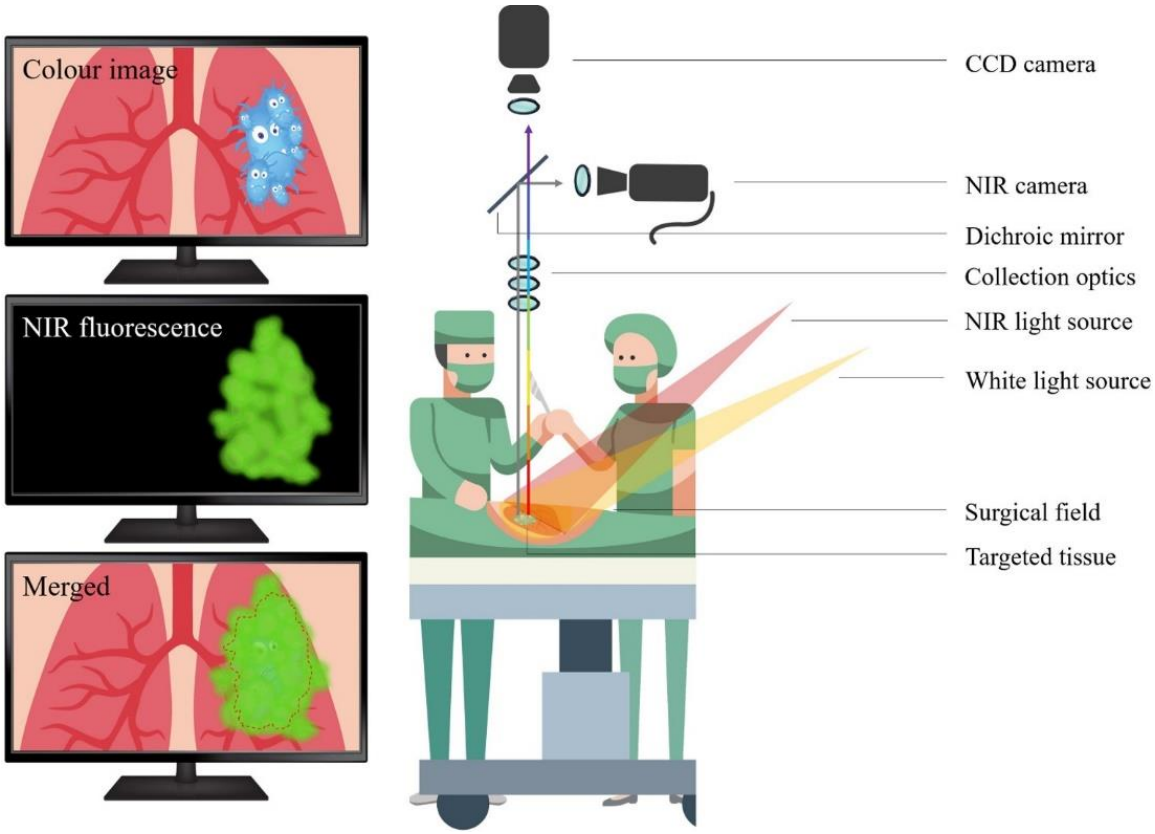

Scheme 1.2. Schematic representation of a surgical field and NIR fluorescence imaging system, capturing simultaneously and in real-time two imaging channels.

Set side-by-side with other classical imaging techniques, fluorescence imaging technique (**Scheme 1.2**) is used for the detection of photons emitted from diseased tissue, after administration of diverse contrast agents of interest, offering high-resolution images, capable of discerning lesions even smaller than 10 μm.

Chapter 2. Brief review on next generation of fluorophore-loaded protein-based nanoparticles for interventional NIR fluorescence imaging of cancer

2.1 Why is NIR so desired?

The use of dyes that both absorb and emit light in the red and NIR region of the spectrum was the stepping stone to overcome the main drawbacks (e.g., the absorption by tissue and blood, scattering of light, autofluorescence of tissue) that limited fluorescence imaging in the ultraviolet-visible (UV-Vis) region to the qualitative surface imaging of only single cell and thin tissue layers. While proteins, melanin, haemoglobin and water have high absorbance coefficients over almost the entire UV-Vis spectrum 200 – 650 nm [20], and collagen absorbs at wavelengths over 1450 nm [20], the tissue penetration of light is highest (up to 2 cm [8]) in the 650 – 1450 nm range of the electromagnetic spectrum, also known as the *optical window* in biological tissue. Hence, in the past years, NIR fluorescence imaging and photoactive agents employed in pre-clinical research gained mass attention globally [6,20].

Organic dyes are the first option as NIR contrast agents for biomedical imaging, and most of them can be catalogued as squaraines, BODIPY, porphyrins, phthalocyanines or cyanines [20,21]. The governing fluorophores and *gold standard*, namely ICG, of successful *in vivo* applications continue to belong to the popular family of ***cyanines***. The first cyanine dye ever synthesized was described as *a blue solid* by Williams in 1856 and, since then, these dyes have been used in a broad range of applications from paints to medicinal purposes.

2.2 Employment of nanotechnology in biomedical applications

To surmount the shortcomings of administrating free dyes e.g., hydrophobicity, aggregation, poor quantum yield and low photostability, an up-and-coming approach is the efficient encapsulation or conjugation of the fluorescent agents (**Scheme 2.1**) with diverse nanoparticles (NPs) [21,22].

Thus, over the past years, researchers delved into the implementation of NPs as personalized contrast and therapeutic agents for medical imaging and phototherapy, owing to their ability to efficiently load and thus overcome the drawback of using free NIR phototheranostic agents[23,24]. Furthermore, some NPs with diameters in the optimal size range can cross the blood brain barrier with ease[24] and have the capability to accumulate preferentially within tumour microenvironments, either through passive targeting mediated by the EPR effect or via active targeting by bioconjugation with cancer-specific ligands[24,25]. On the other hand, in spite of the considerable amount of research carried out for a better understanding of the interplay between synthetic NPs and biological systems, merely a narrow percentage, 2%, reached clinical translation [14]. Thus, an

appealing alternative to synthetic NPs is the employment of the versatile, nontoxic and biodegradable protein-based NPs loaded with NIR fluorophores as medical imaging agents[14,23].

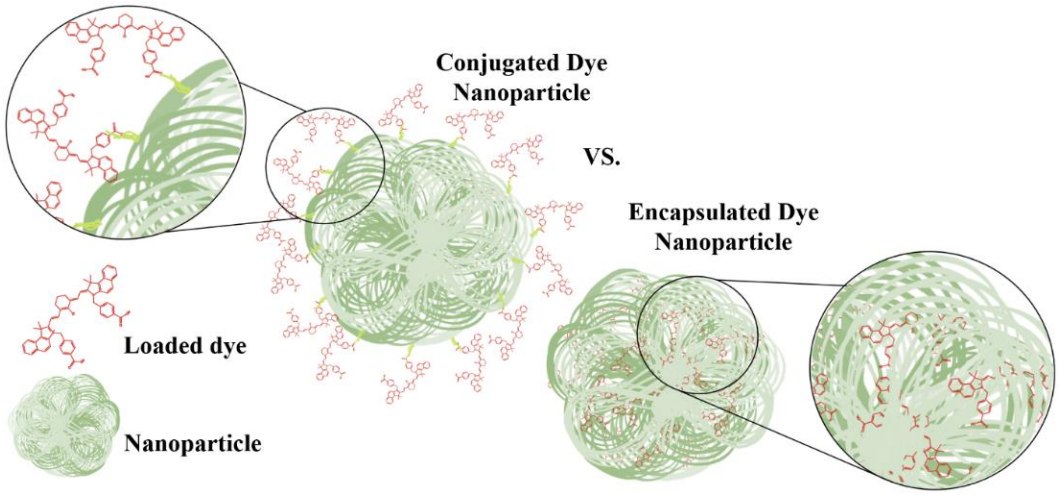

Scheme 2.1. Schematic representation of Conjugated vs. Encapsulated protein-based NPs with NIR emitting fluorophores.

2.3 Protein-based nanoparticles

Up to date ***albumin*** remains the cornerstone of protein-based NPs, thanks to its biodegradability, biocompatibility and capacity to bind to a wide range of dyes, drugs, photosensitizers and other bioactive compounds [24,26]. Albumin is the most abundant of the plasma proteins and for commercial purposes albumin can be derived from egg white, rat serum, bovine serum (bovine serum albumin (BSA)) and human serum (the FDA approved human serum albumin (HSA)). Considering the similitude between the two heart-shaped proteins BSA (583 amino acids, 69.3 kDa molecular weight) and HSA (585 amino acids, 66.5 kDa molecular weight), a large number of bovine and human albumin-based NPs are currently tested in clinical trials [23,26]. Albumin-based NPs gained popularity as contrast agents for medical imaging too, since they are able to encapsulate or conjugate to a large spectrum of dyes. A widely studied NIR contrast agent for the fluorescence imaging of a broad variety of cancer types are the versatile, biocompatible, and biodegradable ICG-loaded HSA NPs. These albumin-based NPs have been designed in different sizes and have been functionalized with various ligands in order to optimize and study *in vivo* and *in vitro* their targeting and delivering performances and offer the possibility of better and personalized treatments in the near future. Chen et al. [27] and Sheng et al. [28] investigated the *in vivo* tumour accumulation and biodistribution of ICG-loaded HSA NPs intravenously injected into nude mice bearing tumours, after being subcutaneously injected with 4T1 cells (murine mammary carcinoma). Both studies reported a prolonged blood circulation half-life of ICG-loaded HSA NPs compared to the

half-life of free ICG, probably mediated by the EPR effect considering the increased sizes of the HSA-based NPs correlated to the size of the free dye molecules.

At last, the emerging need of implementing in clinical trials a new generation of phototheranostic agents for a better intratumoural internalization of the drug of interest and higher tumour to background ratio during surgery, based on the same NIR molecules or new ones, but loaded within nanostructures such as NPs, is undeniable. Moreover, it is worth bearing in mind that out of over 60 NPs that are now approved by the FDA in clinical trials [29], most of the NPs involved in clinical studies in oncology are organic NPs [30]. Thus, with diameters in the optimal range (10-300 nm[31]) to undergo EPR-mediated passive targeting, a versatile surface chemistry offering the possibility of active targeting of the tumours, and countless preclinical studies proving their biocompatibility and efficiency as fluorescent agents, NIR fluorescent protein-based NPs exhibit bright potential as contrast agents for the real-time NIR fluorescence imaging of cancer in clinical trials.

This review was published in International Journal of Nanomedicine, 16 (March 2021): 2147–71.

Part II. Original contributions

Chapter 3. Design and characterisation of fluorophore-loaded albumin nanoparticles

3.1 Experimental design outline and fluorophore-loaded albumin nanoparticles fabrication

In the current clinical context, where significant effort is invested in the development and optimization of fluorescence imaging contrast agents and phototherapeutic agents as well, in view of their implementation in relevant medical applications, the purpose of my doctoral thesis is to design state of the art nanosized agents for the real-time imaging and/or PTT and PDT of cancer. To overcome the drawbacks of using free dyes in systemic administration, such as aqueous-instability, short circulation time, rapid photo-degradation and low fluorescence quantum yields, the aim of my doctoral thesis is to subsequently design protein NPs, precisely BSA and HSA proteins, loaded with four different selected dyes with optical responses from the Vis to the NIR region of the electromagnetic spectrum. Precisely, we fabricated highly reproducible fluorophore-loaded protein NPs (**Scheme 3.1**) following a modified and adapted two-step procedure: i) desolvation using an organic solvent, ethanol, and ii) stabilization by chemical cross-linking with glutaraldehyde (Gal) [32,33].

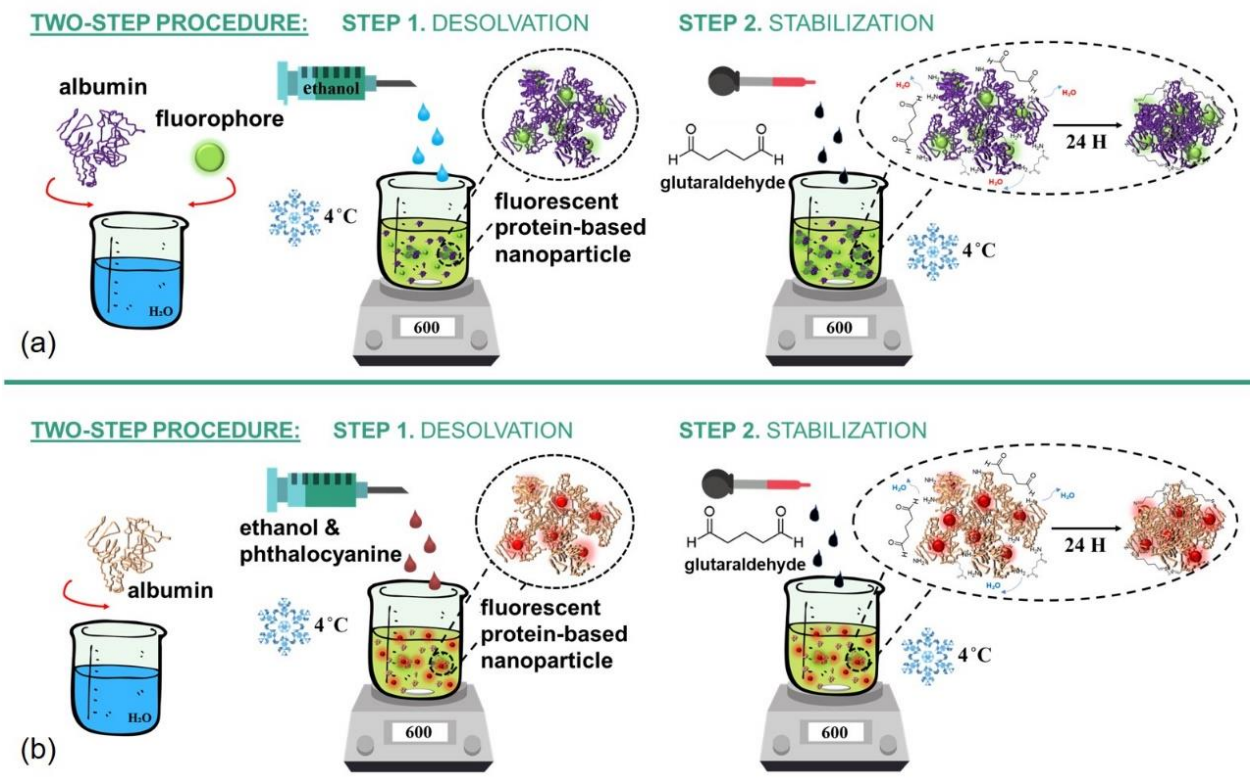

Scheme 3.1. Schematic representation of the two-step synthesis of fluorescent albumin-based NPs**.**

Specifically, since fluorescent-guided surgery may be a feasible instrument in the near future for the real-time detection of different cancer types [8], two FDA approved fluorescent dyes, namely FITC (emission maximum: 522 nm) and ICG (emission maximum: 811 nm), have been employed herein for loading within albumin NPs. Going further, the phthalocyanine moiety is a versatile building block in the design of promising second-generation photosensitizers [34] for photodynamic [35] and photothermal [36] therapy. Compared to other deep red / NIR fluorophores, phthalocyanines exhibit excellent chemo- and photostability, low toxicity in the absence of light, good quantum yield of $^1O_2$ generation [37], but, their principal limitation is the low solubility and aggregation tendency in water. Thus, to suppress the shortcomings of administering phototheranostic agents in their free state, the newly synthesised phthaloNO$_2$ (emission maximum: 690 nm) and phthaloNH$_2$ (emission maximum: 796 nm) molecules have been encapsulated within albumin NPs for further fluorescence imaging and multimodal therapeutic applications. The two phthalocyanine dyes were selected because, in their free form, the fine equilibrium between the three intrinsic functions of the NIR molecules allows them to act at the same time as a photosensitive, thermal and contrast agent. In the following sections, we focused on the design and characterization of the FITC loaded HSA NPs (hereinafter denoted as HSA&FITC NPs), phthaloNO$_2$ loaded HSA NPs (hereinafter

denoted as HSA&phthaloNO$_2$ NPs), ICG loaded HSA NPs (hereinafter denoted as HSA& ICG NPs) and phthaloNH$_2$ loaded BSA NPs (hereinafter denoted as BSA&phthaloNH$_2$ NPs). Next, we decorated the afresh synthesized NPs with ovarian cancer ligands, and *in vitro* studies were carried out. Their biomedical applications, precisely the interventional fluorescence imaging and multimodal therapeutic effect of the albumin NPs were studied in vitro and within murine models.

3.2 Spectroscopic characterization

The absorption maximum bands of FITC reveal clear sensitivity of the dye to the micro-environment, as **figure 3.1 (a)** depicts. When encapsulated within HSA solution, a bathochromic shift of the FITC absorbance band can be observed prior to stabilization with Gal of HSA&FITC NPs (absorption maximum at 498 nm), while for the final HSA&FITC NPs (absorption maximum at 491 nm) a hypsochromic shift can be noted, compared with the free FITC solution (absorption maximum at 494 nm).

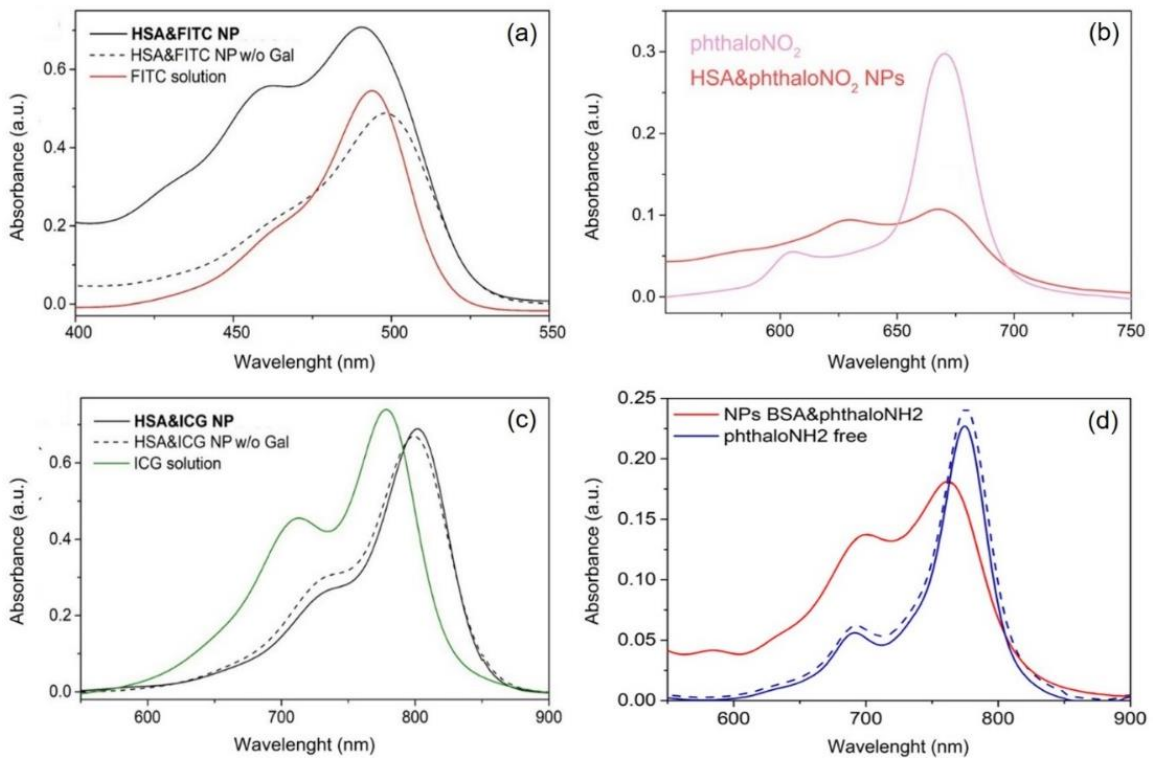

Figure 3.1. Absorbance spectra of (a) free FITC solution (red) and HSA&FITC NPs before (dash line) and after (solid line) stabilization with Gal; (b) free phthaloNO$_2$ solution (pink) and HSA&phthaloNO$_2$ NPs; (c) free ICG solution (green) and HSA&ICG NPs before (dash line) and after (solid line) stabilization with Gal; and (d) free phthaloNH$_2$ solution (blue) and HSA&phthaloNH$_2$ NPs, at 25 ºC (dash line) and at 37 ºC (solid line).

Another indicator for the formation of fluorescent HSA NPs in aqueous solution is the Rayleigh scatter present in the blue region of the HSA&FITC NPs absorbance spectrum. The emission peak of free FITC solution (emission maximum at 522 nm) showed 2, respectively 3 nm bathochromic shifts in comparison to HSA&FITC NPs without (w/o) Gal (emission maximum at 524 nm) and HSA&FITC NPs (emission maximum at 525 nm) (**Figure 3.2 (a)**).

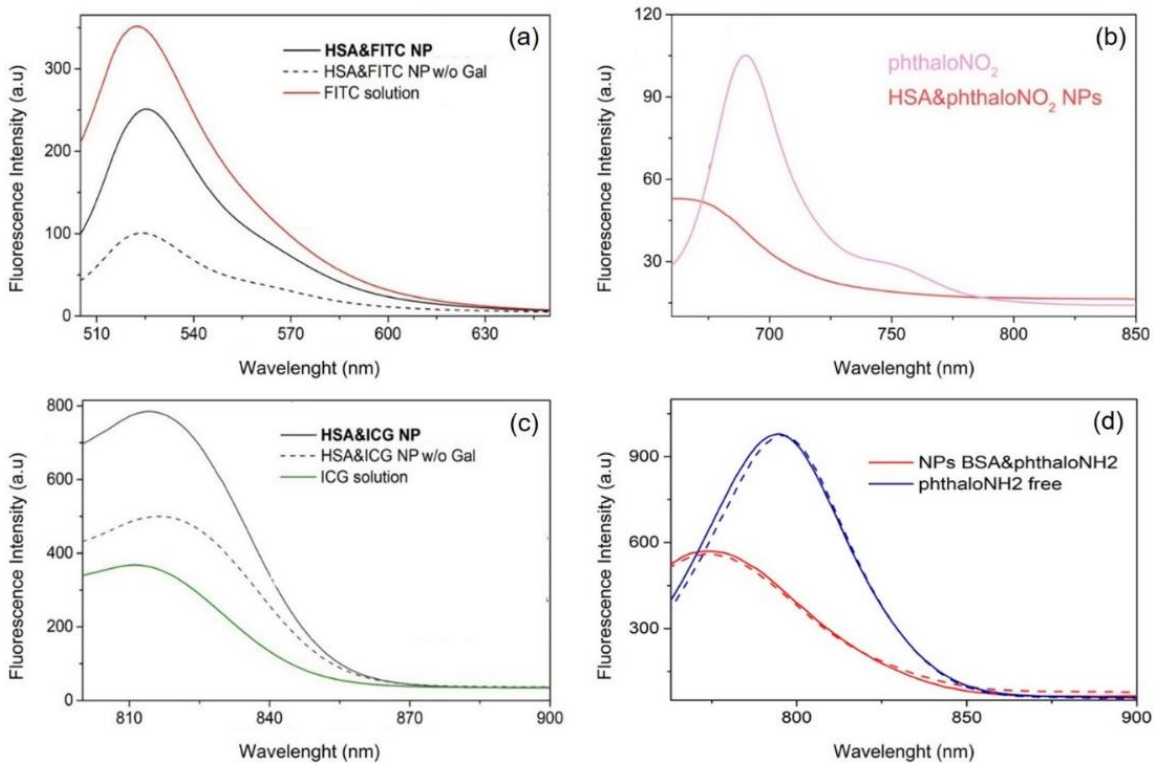

Figure 3.2. Steady-state fluorescence emission spectra of (a) free FITC solution (red) and HSA&FITC NPs before (dash line) and after (solid line) stabilization with Gal; (b) free phthaloNO$_2$ solution (pink) and HSA&phthaloNO$_2$ NPs; (c) free ICG solution (green) and HSA&ICG NPs before (dash line) and after (solid line) stabilization with Gal; and (d) free phthaloNH$_2$ solution (blue) and HSA&phthaloNH$_2$ NPs, at 25 ºC (dash line) and at 37 ºC (solid line).

In parallel with the above-mentioned synthesized fluorescent HSA NPs, the formation of the HSA&phthaloNO$_2$ NPs was confirmed by a small 2 nm hypsochromic shift in the absorbance spectra (**Figure 3.1 (b)**) and 27 nm blue shift for the fluorescence emission spectra (**Figure 3.2 (b)**) of the phthaloNO$_2$ after encapsulation within the HSA NPs. A significant modification in the aspect of the phthaloNO$_2$ absorbance spectra can be observed before and after encapsulation, suggesting a susceptible behavior of the molecule to changes in its immediate environment. Moreover, the decrease in the

fluorescence intensity and hypsochromic shift of the phthaloNO$_2$ fluorophore after the formation of the HSA NPs indicate the loading of the fluorophore within the HSA protein.

Considering that the photophysical behaviour of the ICG dye can be easily influenced by changes in the environment, after the formation of the HSA&ICG NPs, the fluorescence intensity of the complex was highly increased (**Figure 3.2 (c)**) as a result of the 24 nm bathochromic shift (**Figure 3.1 (c)**) of the HSA&ICG NPs absorbance band attributed to the ICG (absorption maximum at 802 nm) in respect to the absorbance band of free ICG solution in water (absorption maximum at 778 nm). Similar to ICG, although there is only a 3 nm red shift (**Figure 3.1 (c)**) observed between the absorbance band of HSA&ICG NPs w/o Gal (absorption maximum at 799 nm) and HSA&ICG NPs, there is a notable increase in the fluorescence intensity of HSA&ICG NPs (emission maximum at 814 nm) by comparison with HSA&ICG NPs w/o Gal (emission maximum at 816 nm) (**Figure 3.2 (c)**), indicating a more favourable configuration of the fluorophore inside the HSA NPs after stabilization by chemical cross-linking with Gal.

Next, we wanted to compare the free phthaloNH$_2$ with the previously synthesized BSA&phthaloNH$_2$ NPs at room temperature, 25 ºC, and at a biologically relevant temperature, 37 ºC, to confirm their adaptability in biomedical applications. In the absorbance (**Figure 3.1 (d)**) and fluorescence emission (**Figure 3.2 (d)**) spectra we presented spectra measurements both at 25 ºC and 37 ºC. We can observe that that the absorption and the emission maximum of BSA&phthaloNH$_2$ NPs does not shift once the temperature is increased, remaining preserved both at 25 ºC (dashed line) and 37 ºC (solid line). Following the same pattern, the absorbance spectra (**Figure 3.1 (d)**) of the free phthaloNH$_2$ has the exact same absorption maximum at 25 ºC (dashed line) as at 37 ºC (solid line), precisely 775 nm, but we ca see a slight decrease in intensity as the temperature rises. BSA&phthaloNH$_2$ NPs fluorescence emission undergoes changes compared to free phthaloNH$_2$ because of the environmental change of the phthaloNH$_2$ molecules immediate surrounding once encapsulated within the BSA NPs.

3.3 Physical properties and particle yield

As delineated in **figure 3.3**, the dry sizes of the newly synthesized fluorophore-loaded albumin NPs revealed by TEM investigations are in consonance with the average hydrodynamic diameters of the albumin NPs established by Dynamic Light Scattering (DLS) measurements (**Table 3.1**). All four types of fluorophore-loaded albumin NPs presented negative charged surfaces as revealed by zeta-potential measurements (**Table 3.1**). Going further, as already suggested in the schematic representation of the two-step synthesis of the fluorescent NPs in **scheme 3.1**, Gal was used as an aggressive carbonyl reagent that condenses amines, leading to a decrease of 69.3% and 69.4% in the diameters of the HSA&FITC and HSA&ICG NPs and a decrease of 2.5, respectively 4.3 mV in the zeta-potential measurements. These results are summarized in **table 3.1**.

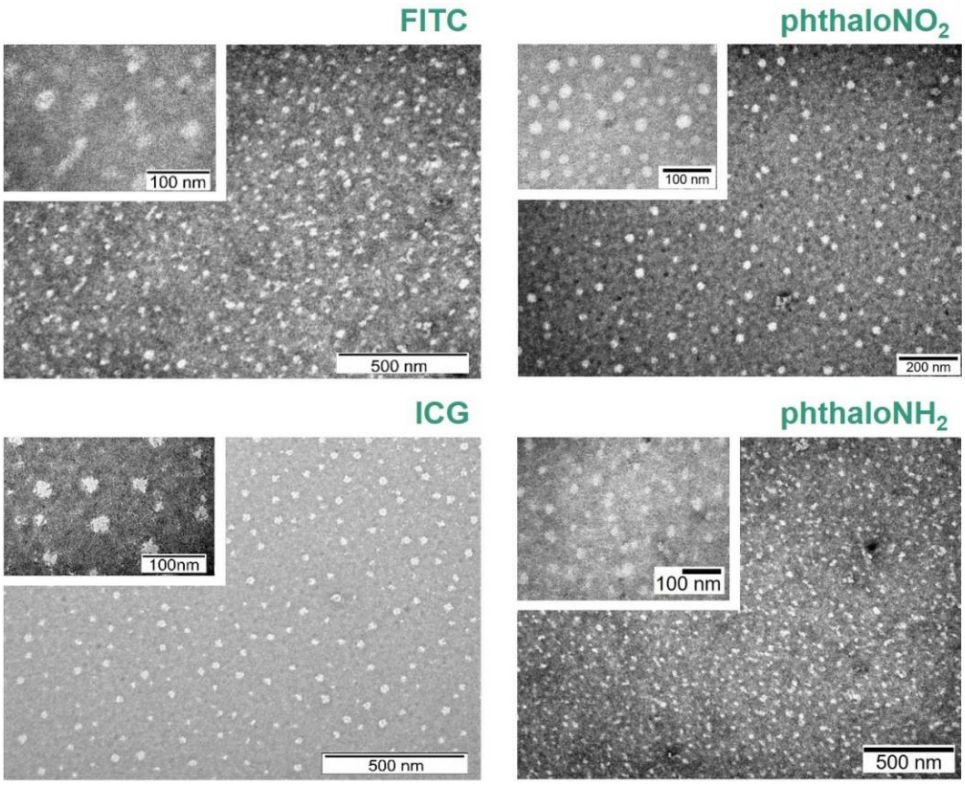

Figure 3.3. Representative TEM images of HSA&FITC, HSA&phthaloNO$_2$, HSA&ICG and BSA&phthaloNH$_2$ NPs, at lower and higher magnifications.

Table 3.1. Zeta-potential and DLS data of HSA&FITC, HSA&phthaloNO$_2$, HSA&ICG and BSA&phthaloNH$_2$ NPs.

	zeta-potential (mV)	diameter (nm)	PDI	decrease in diameter after stabilization with Gal (%)
HSA&FITC NPs	-12.9 ± 0.4	31.26 ± 0.53	0.23 ± 0.01	69.3
before stabilization with Gal	-10.4 ± 0.2	101.40 ± 2.12	0.23 ± 0.01	
HSA&phthaloNO$_2$ NPs	-13.8 ± 1.2	21.3 ± 0.20	0.19 ± 0.02	–
HSA&ICG NPs	-15.1 ± 1.6	25.86 ± 0.17	0.25 ± 0.01	69.4
before stabilization with Gal	-10.8 ± 0.2	84.85 ± 1.18	0.23 ± 0.01	
BSA&phthaloNH$_2$ NPs	-12.6 ± 0.9	28.54 ± 0.42	0.19 ± 0.03	–

To calculate the particle yield of the afresh designed fluorophore-loaded albumin NPs, a calibration curve was established for albumin solutions of different concentrations (1, 2, 3, 4 and 5%) and their absorbance optical density recorded at 277 nm. The stock solutions used for the serial dilutions of the standard albumin aqueous solutions had the same concentrations as the stock solutions used in the synthesis of the fluorophore-loaded albumin NPs. The particle yields of the albumin NPs was calculated as percentage of the initial concentration of the protein. These results (**Table 3.2**) confirm the great particle formation rates, along with the good reproducibility of the synthesis. Standard errors were calculated for measurements recorded in triplicate.

Table 3.2. Particle yield of HSA&FITC NPs, HSA&phthaloNO$_2$ NPs, HSA&ICG NPs and BSA&phthaloNH$_2$ NPs.

	FITC	phthaloNO$_2$	ICG	phthaloNH$_2$
Particle yield (%)	77.6 ± 4.1	73.7 ± 3.9	77.9 ± 6.1	75.8 ± 1.3

3.4 Albumin-dye interplay and loading efficiency

Afterwards, calibration curves were established for the four different fluorophores solutions of different concentrations (FITC@PBS (7x10^{-6} to 10^{-4} M), phthaloNO$_2$@DMSO (7.5 x 10^{-7} to 2.5 x 10^{-5} M), ICG (10^{-6} to 10^{-4} M) and phthaloNH$_2$@DMSO (7.5 x 10^{-7} to 2.5 x 10^{-5} M)) and their absorbance optical density recorded at 504 nm for FITC, 672 nm for phthaloNO$_2$, 795 nm for ICG and 774 nm for phthaloNH$_2$, respectively. The stock solutions used for the serial dilutions of the standard dye solutions had the same concentrations as the stock solutions used in the synthesis of the albumin NPs. We determined the FITC and ICG loading efficiency by solving **equation 3.1**, while the loading efficiency of phthaloNO$_2$ and phthaloNH$_2$ was calculated by solving **equation 3.2**. These results (**Table 3.3**) affirm the high amount of the four dyes confined within the albumin NPs and, undoubtedly, the excellent loading efficiency of our albumin NPs. To calculate the standard error, the measurements were recorded in triplicate.

$$loading\ efficiency\ (\%) = \frac{amount\ of\ dye\ in\ NPs}{initial\ amount\ of\ dye} \times 100 \quad (\mathbf{3.1})$$

$$loading\ efficiency\ (\%) = \frac{initial\ amount\ of\ dye - amount\ of\ dye\ in\ pellet}{initial\ amount\ of\ dye} \times 100 \quad (\mathbf{3.2})$$

Table 3.3. Dye loading efficiency of HSA&FITC NPs, HSA&phthaloNO$_2$ NPs, HSA&ICG NPs and BSA&phthaloNH$_2$ NPs.

	FITC	phthaloNO$_2$	ICG	phthaloNH$_2$
Loading efficiency (%)	31.4 ± 3.1	87.8 ± 0.2	49.8 ± 4.5	91.1 ± 1.5

The newly synthesized phthalocyanine dyes were developed by colleagues from The Research Centre on Fundamental and Applied Heterochemistry Faculty of Chemistry and Chemical Engineering, Babes Bolyai University, Cluj-Napoca, Romania.

Research results presented in this chapter have been published in Nanotechnology, 31, no. 31 (July 2020): 315102, Biomaterials Science, 9 (July 2021): 6183-6202 and Molecules, 26(15) (August 2021): 4679, Journals.

Chapter 4. Targeting and cellular uptake of newly fabricated fluorophore-loaded protein-based nanoparticles by ovarian cancer cells

4.1 Biofunctionalization of the nanoparticles with ovarian cancer-specific ligands

While the delivery of NPs without specific targeting elements is based on EPR-mediated passive targeting, a more efficient tumour cell internalization could be obtained by active targeting based on biofunctionalization of the NPs with specifically selected ligands. Thus, the fluorophore-loaded HSA NPs have been covalently conjugated either with folic acid (FA) molecules or anti-FRα antibody proteins (hereinafter denoted as AB), in order to bind specifically to the FRα protein overexpressed on most ovarian cancer cells. The biofunctionalization with FA and AB was carried out following the well-known N-(3-Dimethylaminopropyl)-N'-ethyl carbodiimide hydrochloride (EDC) / N-hydroxysuccinimide (NHS) activation mechanism. Control sample were prepared following the same protocol as for the biofunctionalization of the fluorescent HSA NPs, but without the addition of the activated FA and AB.

4.2 Characterization of active targeting fluorophore-loaded nanoparticles in solution

The hydrodynamic diameter of the control fluorescent HSA&FITC NPs, 25.18 ± 0.20 nm and PDI 0.22 ± 0.01, increased with about 9 nm once the FA was covalently conjugated to the HSA&FITC NPs (hereinafter denoted as HSA&FITC-FA NPs), 33.70 ± 0.29 nm and PDI 0.23 ± 0.01 (**Table 4.1**).

Table 4.1. Zeta-potential and DLS data of HSA&FITC–FA NPs, HSA&phthaloNO$_2$–FA NPs and HSA&ICG–FA NPs.

	HSA&FITC NPs		HSA&phthaloNO$_2$ NPs		HSA&ICG NPs	
	with targeting	without targeting	with targeting	without targeting	with targeting	without targeting
diameter (nm)	33.7 ± 0.3	25.2 ± 0.2	28.3 ± 1.2	21.3 ± 0.2	26.6 ± 0.2	22.3 ± 0.3
increase in diameter (nm)	8.5		7.0		4.3	
PDI	0.23 ± 0.01	0.22 ± 0.01	0.32 ± 0.05	0.19 ± 0.02	0.24 ± 0.01	0.31 ± 0.01
zeta-potential (mV)	-18.0 ± 0.5	-15.3 ± 2.6	-9.4 ± 0.2	-13.8 ± 1.2	-14.2 ± 0.8	-12.9 ± 0.6
difference in zeta-potential (mV)	2.7		4.4		1.3	

Since the activated FA was conjugated to the fluorescent HSA NPs through the amino groups located at the surface, and FA has at the distal end an amino group as well, no major differences were observed between the zeta-potentials of the control HSA&FITC NPs, -15.3 ± 2.6 mV, and HSA&FITC-FA NPs, -18.0 ± 0.5 mV (**Table 4.1**). Next, having a final average hydrodynamic diameter of 28.3 ± 1.2 nm and PDI of 0.32 ± 0.05 (**Table 4.1**), the 7 nm increase in size of the HSA&phthaloNO$_2$-AB NPs stands as proof that the HSA&phthaloNO$_2$ NPs were successfully decorated with AB. Since the pH of the surrounding medium, namely PBS (pH 7.4), is very close to the isoelectric point of AB [38], and, implicitly, the net charge of AB is near zero, it is no wonder that only a slight change was noticed in the zeta-potential (**Table 4.1**) of the HSA&phthaloNO$_2$ NPs once biofunctionalized with AB (HSA&phthaloNO$_2$-AB NPs zeta-potential: -9.4 ± 0.2 mV). Finally, similarly to the behaviour observed for the HSA&FITC-FA NPs, the hydrodynamic diameter of the control HSA&ICG NPs, 22.31 ± 0.34 nm and PDI 0.31 ± 0.01, increased with approximately 5 nm once the activated FA was covalently conjugated to the HSA&ICG NPs (hereinafter denoted as HSA&ICG-FA NPs), 26.63 ± 0.22 nm and PDI 0.24 ± 0.01. No significant differences were observed between the zeta-potentials of control the HSA&ICG NPs, -12.9 ± 0.6 mV, and the HSA&ICG-FA NPs, -14.2 ± 0.8 mV (**Table 4.1**).

Moreover, the HSA&FITC-FA and HSA&ICG-FA NPs present excellent size stability and fine photostability after the first week of the trial, whereas the fluorescence intensity of HSA&ICG-FA NPs is maintained, even increased, at the end of the 15-day trial period, 111.2% for HSA&ICG NPs and 91.6% of the initial fluorescence intensity for HSA&FITC NPs (**Figure 4.1**). DLS data of fresh and one-month old fluorescent HSA-FA NPs indicate excellent stability regarding their size, with a negligible increase of 1 nm for the HSA&ICG-FA NPs (28.40 ± 0.17 nm and PDI 0.23 ± 0.02 – after 1 month), and an increase of 3 nm for HSA&FITC-FA NPs, respectively (37.15 ± 0.06 nm and PDI 0.30 ± 0.01 – after 1 month). Overall, even though both dye solutions tend to lose their fluorescence

characteristics in time, the free FITC solution shows more stable fluorescence properties over time compared to free ICG solution. However, when encapsulated in HSA NPs, the fluorescence characteristics of the two dyes are maintained, or even amplified for the HSA&ICG-FA NPs.

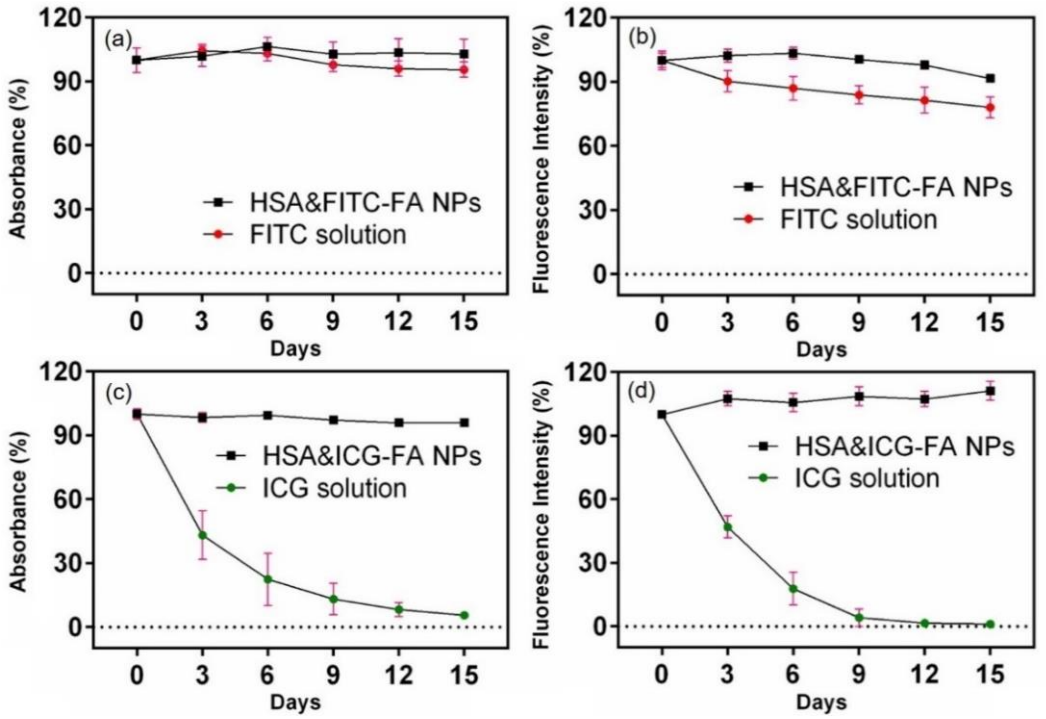

Figure 4.1. Absorbance – (a) and (c) – and fluorescence intensity measurements – (b) and (d) – over a period of 15 days for free ICG (green dots) and free FITC (red dots) solutions in comparison with the fluorescent HSA-FA NPs (black squares), represented as percentages of the initial fluorescence.

4.3 Cell viability assay

The first step towards the translation of the four studied types of fluorophore-loaded albumin NPs to *in vivo* studies was to confirm their *in vitro* biocompatibility upon treatment of three ovarian cancer cell lines (NIH:OVCAR3, A2780 and A2780 Cis), by employing the *gold standard* of cell viability assay, namely the MTT assay. Although the free phthaloNO_2 and phthaloNH_2 solutions reduced the viability of the treated cells in a concentration-dependent manner, after encapsulation all four classes of fluorophore-loaded albumin NPs showed no cytotoxic effects.

4.4 Cellular uptake by fluorescence microscopy

Fluorescence microscopy images were acquired for a better perspective on the cellular uptake of the FA targeted and untargeted HSA&FITC NPs (**Figure 4.2**). Thus, we can

confirm the enhanced cellular uptake for the HSA&FITC-FA NPs, thanks to the biofunctionalization of the albumin NPs with ovarian-cancer targeting molecules.

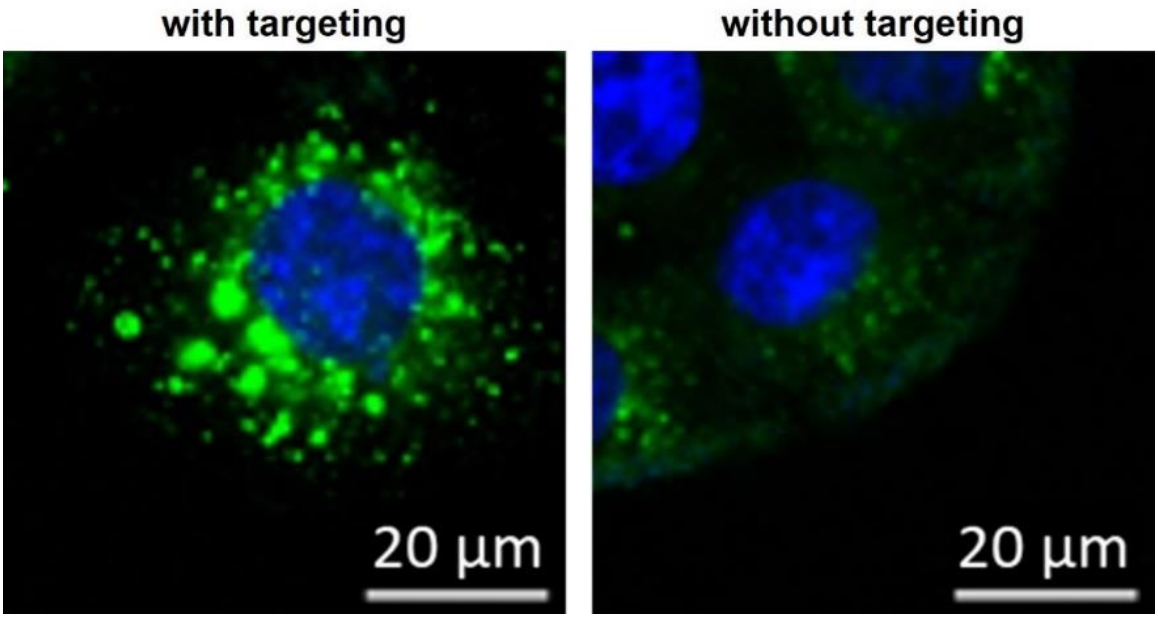

Figure 4.2. Fluorescence Microscopy Imaging of the NIH:OVCAR3 cells treated with targeted (left) and untargeted (right) HSA&FITC NPs. The cells were stained with DAPI (blue).

4.5 Cellular uptake by TEM

To go further into the mechanism of cellular uptake of HSA NPs, *in vitro* TEM investigations were performed (**Figure 4.3**). The cells treated with HSA NPs had comparable ultrastructure as the other groups, including the high number of organelles and autophagosomes (**Figure 4.3 (c)**). We also found the NP-containing vesicles in the cells of this group (inset of **figure 4.3 (c)**), but the NPs seemed to be smaller and less numerous, and the NP-containing vesicles themselves were found in a lower number of cells compared to the group of cells treated with HSA-FA NPs. The NP-containing vesicles were identified again in the cells treated with FA + HSA-FA NPs – competitive control group (**Figure 4.3 (d)**). However, in the cells of this group these vesicles were smaller compared to those observed in the cells of the other treated groups, and the NPs were also less densely packed inside them (inset of **figure 4.3 (d)**).

These results validate once again the enhanced internalization of HSA-FA NPs due to their efficient targeting of the FRα overexpressed on NIH:OVCAR3 cells.

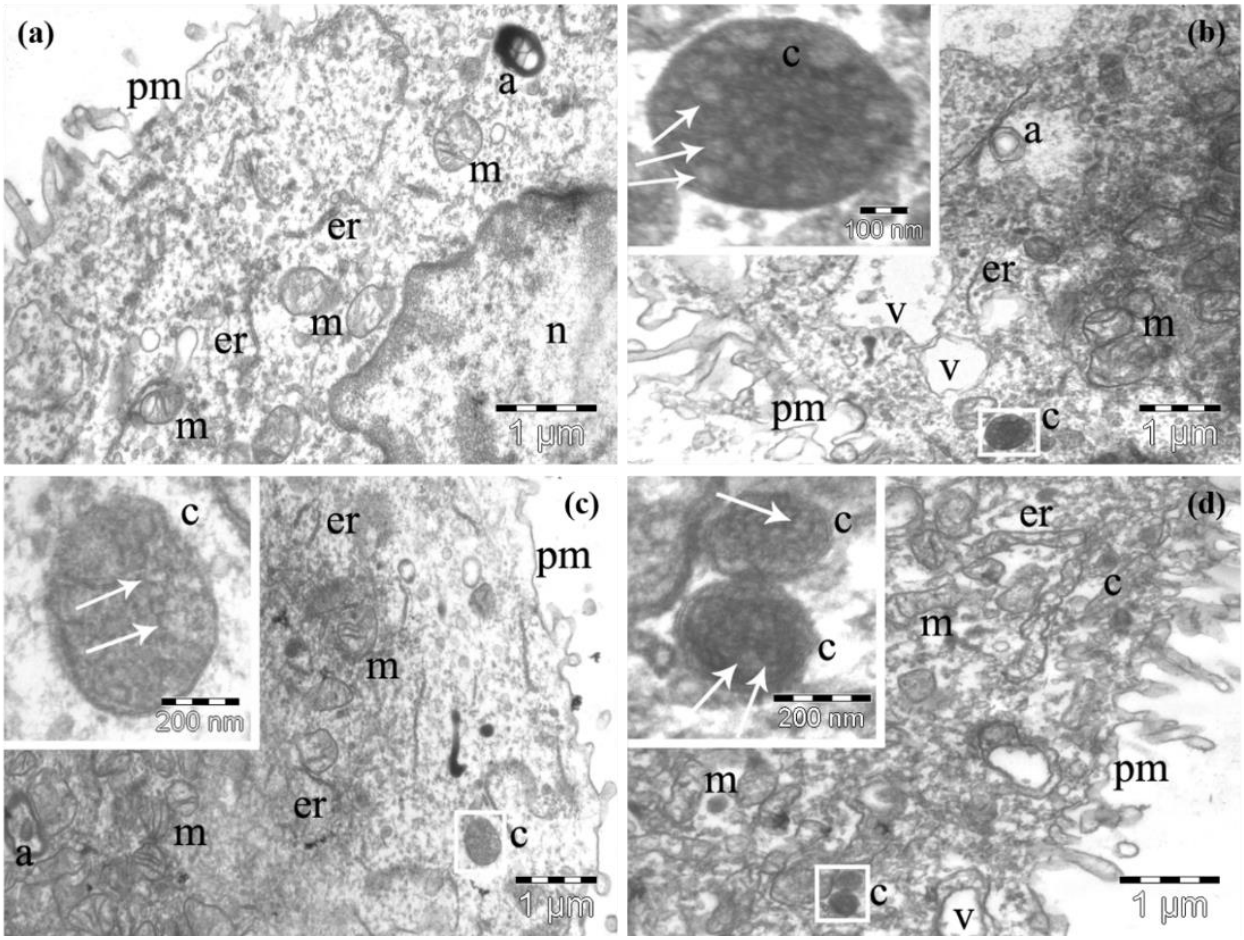

Figure 4.3. TEM images of the NIH:OVCAR3 cells in the four different groups. Untreated cell from the control group with characteristic aspect (a). The NPs were located inside caveosomes within the cells treated with HSA-FA NPs (b), with HSA NPs (c), and with FA + HSA-FA NPs (d). The presence of the NPs inside the caveosomes was highlighted with increased magnification in the corresponding insets of panels (b-d). a – autophagosomes; c – caveosomes; er – endoplasmic reticulum; m – mitochondria; n – nucleus; pm – plasma membrane; v – vacuoles

All in vitro studies were performed in collaboration with the Department of Radiobiology and Tumor Biology, Oncology Institute "Prof. Dr. Ion Chiricuta", Cluj-Napoca, Romania.

Research results presented in this chapter have been published in Nanotechnology, 31, no. 31 (July 2020): 315102, Biomaterials Science, 9 (July 2021): 6183-6202 and Molecules, 26(15) (August 2021): 4679, Journals.

Chapter 5. Assessment and validation of the phototherapeutic activity of fluorophore-loaded protein-based nanoparticles

5.1 Phototherapeutic effects: in solution assay

An up-and-coming cancer treatment method is PDT. For this therapy to work, three elements, namely a photosensitizer agent, photosensitizer specific excitation wavelength light and intracellular oxygen are indispensable. If we combine these 3 elements, they produce photochemical reactions that lead to the generation of cytotoxic reactive oxygen species, predominantly $^1O_2$. This ROS can trigger the patients' immune system, can close the vasculature around the tumour and, most important, can cause immediate cancer cells death[3,39]. Another cancer therapy that implies the use of electromagnetic radiations is PTT. When photothermal agents reach an excited state by absorption of photons, they generate heat in order to return to the equilibrium state [12]. Then, if the temperature of 40 °C [40], or above, is reached in their immediate environment, cancer cells are destroyed by thermal ablation [15].

We validated the BSA&phthaloNH$_2$ NPs soupçon capacity to generate $^1O_2$, in solution, resulting in a yield of 6%. The photothermal assay performed in the presence of the BSA&phthaloNH$_2$ NPs was a success, with an increase of 10 ºC after only 15 min of irradiation with the 785 nm NIR laser (photothermal conversion efficiency of 20%), compared to the free phthaloNH$_2$ which increases its temperature with 11 ºC after 9 min of irradiation, but then it reaches a saturation point and by the 15th min of irradiation its temperature is decreased with 2 ºC. The BSA&phthaloNH$_2$ NPs presents great photostability after 3 On/Off irradiation cycles (reaching 67.9% of the maximum temperature recorded in the 1st cycle), compared to the free phthaloNH$_2$ which heats up only to 44.2% of the maximum temperature attained in the 1st cycle (**Figure 5.1 (a)**). Moving forward, the efficiency to convert light-to-heat of the HSA&phthaloNO$_2$ NPs in solution, 2.6%, is close to the values reported in the literature, for the FDA approved ICG. Moreover, a 43% $^1O_2$ quantum yield was calculated for the HSA&phthaloNO$_2$ NPs.

Subsequently, we studied the BSA&phthaloNH$_2$ NPs hydrodynamic diameter before and after irradiation. From **figure 5.1 (b)** we observe that the BSA&phthaloNH$_2$ NPs decreases in intensity after irradiation, but the hydrodynamic diameter remains relatively constant. Before irradiation, the protein-based NPs have a hydrodynamic diameter of 28.54 $\pm$ 0.42 nm and PDI 0.194 $\pm$ 0.027 and after exposure to the NIR laser line, they present a hydrodynamic diameter of 30.66 $\pm$ 1.30 nm and PDI 0.185 $\pm$ 0.062, the insignificant 2 nm increase upholding the good size stability of our BSA&phthaloNH$_2$ NPs.

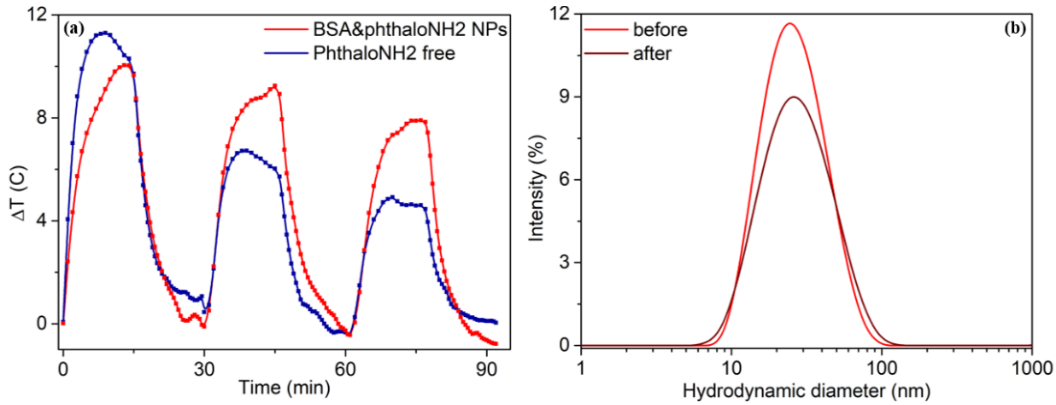

Figure 5.1 (a) The thermal curves of the BSA&phthaloNH$_2$ NPs (red) and of the free phthaloNH$_2$ (blue) obtained after three On/Off irradiation cycles. (b) The DLS spectra presents BSA&phthaloNH$_2$ NPs hydrodynamic diameter stability assay before (red) and after (brown) irradiation.

The photothermal stability of the HSA&phthaloNO$_2$ NPs was evaluated under three heating/cooling cycles (**Figure 5.2**), revealing that after each cycle the maximum temperature value was slightly reduced, by 9% after the second cycle and 20% after the last one, probably due to a mild photodegradation of the phthaloNO$_2$ molecule during the heating cycles.

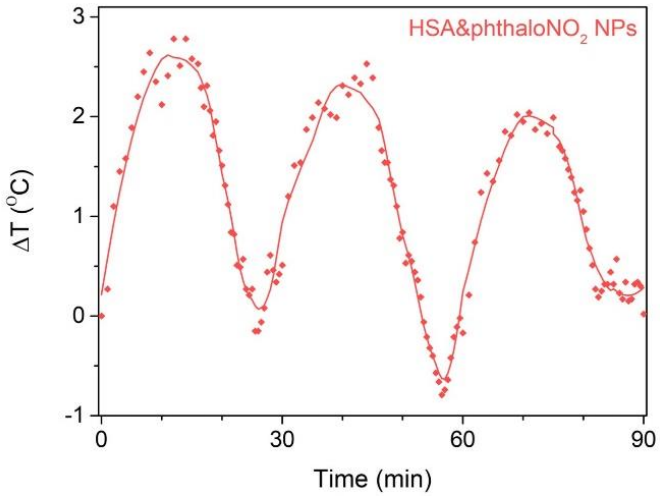

Figure 5.2. Thermal curves in time of HSA&phthaloNO$_2$ NPs during 3 heating/cooling cycles, under irradiation with a 660 nm LED lamp.

The feature of the HSA&phthaloNO$_2$ NPs to protect the phototheranostic agent from denaturation after prolonged exposure to light was assessed by steady-state fluorescence spectroscopy. Fluorescence spectra were acquired before and after 15 min of continuous irradiation with a 660 nm LED lamp for HSA&phthaloNO$_2$ NPs and free phthaloNO$_2$ solution (**Figure 5.3**). The fluorescence intensity of the free phthaloNO$_2$ solution was reduced by 67.1% after exposure to light, whereas the fluorescence of

HSA&phthaloNO$_2$ NPs was decreased only by 30.4%, outlining the enhanced phototherapeutic effects of phthaloNO$_2$ once encapsulated within the HSA NPs.

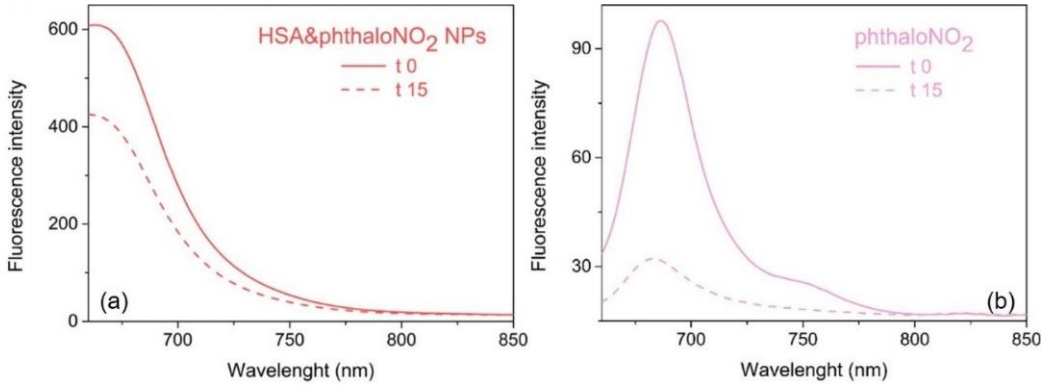

Figure 5.3. Fluorescence emission spectra of (A) HSA&phthaloNO$_2$ NPs and (B) phthaloNO$_2$ solution, at the initial time (solid line) and after 15 min of irradiation (dashed line) with a 660 nm LED lamp.

5.2 Phototherapeutic effects: *in vitro* assay

Next, by exposure of A2780 cells to a 660 nm LED lamp, the *in vitro* multimodal therapeutic effects of the HSA&phthaloNO$_2$-AB NPs were studied by MTT, fluorescence microscopy and flow cytometry assays. In all cases, longer irradiation times resulted in less viable cells, the survival of the cells being influenced in a time dependent manner. MTT analysis (**Figure 5.4**) showed that after 5 min irradiation of the cells treated with HSA&phthaloNO$_2$-AB NPs, the viability of the cells was reduced to 18%, while after 15 min irradiation the viability was only 5%, compared to the control group, thus upholding the high efficiency of these NPs to induce cell death in A2780 cell line after exposure to irradiation.

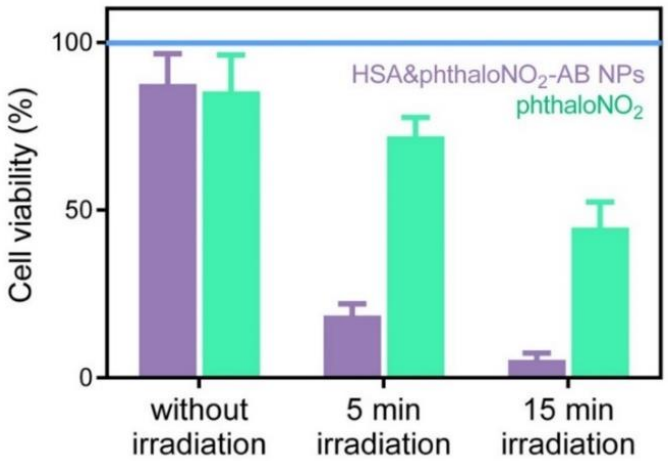

Figure 5.4. MTT assay performed on A2780 cell line to study the multimodal therapy efficiency of HSA&phthaloNO$_2$-AB NPs (violet) and phthaloNO$_2$-solution (green) in the absence of irradiation and after 5 and 15 min of irradiation; control group represented by the blue horizontal line (100% viability).

The treatment with free phthaloNO$_2$ combined with 5 min exposure to irradiation reduced the viability of cells to 72%, and after 15 min exposure to 45%, proving to be less effective in destroying cancer cells compared to the HSA&phthaloNO$_2$-AB NPs. These results are in consonance with the $^1O_2$ quantum yields values calculated in solution for HSA&phthaloNO$_2$ NPs and free phthaloNO$_2$ in section 5.*1*. The control samples kept in the dark at all times (without irradiation) showed negligible change in the viability of cells. Moreover, the MTT assay validates that the survival of the cells is affected in a time dependent manner, longer irradiation times resulting in reduced viability, as expected.

For a better visualization of the synergetic therapeutic effect of HSA&phthaloNO$_2$-AB NPs upon A2780 cells, epi-fluorescence imaging was employed (**Figure 5.5**).

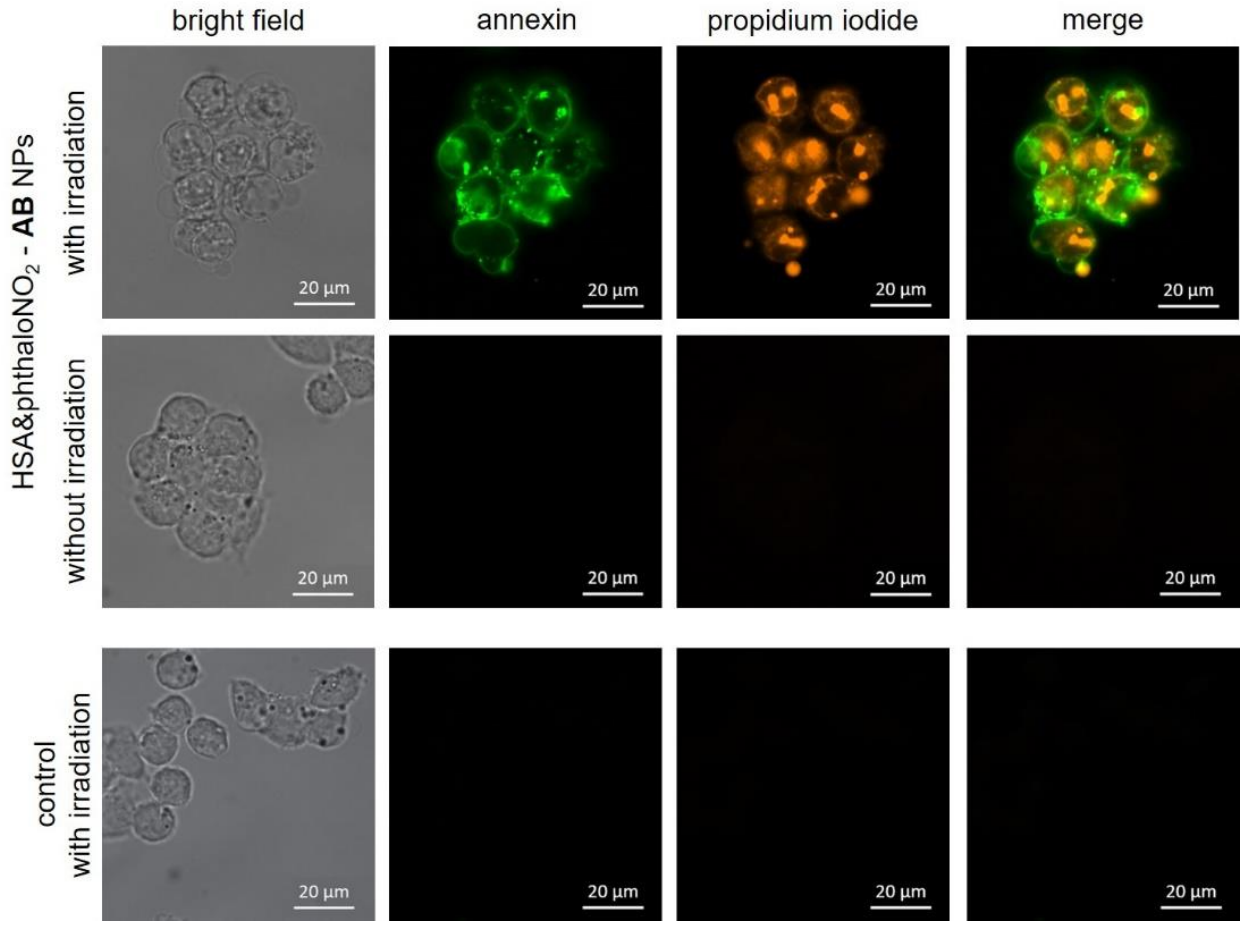

Figure 5.5. Photoinduced therapy studied on A2780 cells treated with HSA&phthaloNO$_2$-AB NPs and an irradiated control group. The cells were stained with Annexin V (green) and PI (orange) and observed under fluorescence or bright field microscopy. Magnification 63x.

Annexin V is a dye able to detect the early event of the apoptotic process, while propidium iodide (PI) stains the nuclei of the cells which have lost the integrity of their plasma membrane, and is a feature characteristic for necrosis. After 4 hours incubation following the treatments, the images show a few cells stained only with Annexin V, excluding PI – apoptotic cells, a few cells positive for PI – necrotic cells and also a small number of cells which were not stained with any of the dyes (viable cells). The majority of the cells were stained with both Annexin V and PI, suggesting that cellular death was induced by apoptosis or necrosis.

Next, to quantify the photoinduced therapeutic effects of the HSA&phthaloNO$_2$-AB and free phthaloNO$_2$, flow cytometric assay was performed. Cells treated with HSA&phthaloNO$_2$-AB NPs were irradiated for 5 and 15 min, respectively, with the 660 nm LED lamp, and after 4h incubation the cells were collected, stained with Vybrant Annexin V-PI apoptosis kit and analysed by flow cytometry (**Figure 5.6**). 5 min of irradiation after treatment with the HSA&phthaloNO$_2$-AB NPs resulted in 6.88% cells showing positivity for Annexin V (apoptotic cells), 14.83% cells were stained with PI (necrotic cells) and 58.78% cells presented double staining (dead cells). 15 min irradiation of the cells treated with HSA&phthaloNO$_2$-AB NPs led to the positivity of 97.43% of the cells, of which only 1.92% for Annexin V, 7.28% for PI and the majority, 88.23% for both Annexin V and PI.

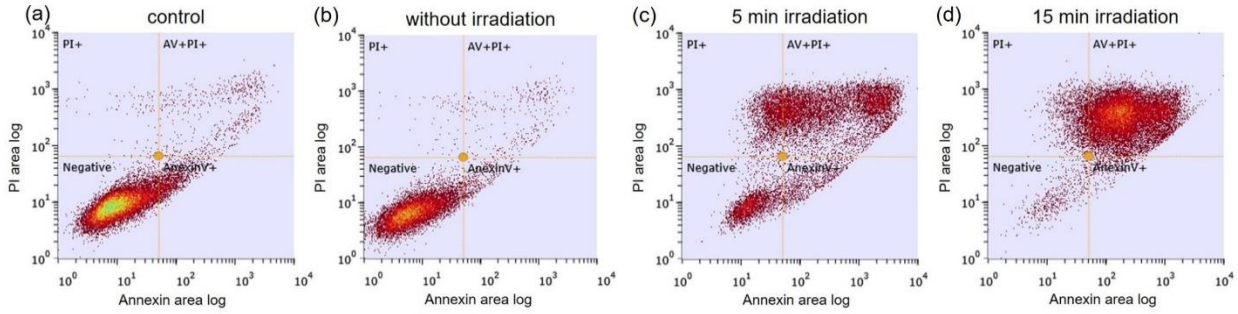

Figure 5.6. Flow cytometry analysis of A2780 ovarian cancer cells (a) without treatment and irradiated for 15 min with a 660 nm LED, and after treatment with HSA&phthaloNO$_2$-AB NPs (b) without irradiation, (c) after 5 min irradiation and (d) after 15 min irradiation. Cells were stained with Annexin V and PI.

These results are well-correlated with those obtained in the MTT test, as well as with the images obtained by fluorescence microscopy, suggesting once again that the combined treatment represents a very efficient modality for the destruction of ovarian cancer cells. Our results are similar to those obtained by Doshi et al. [41], on OVCAR3 ovarian cancer cell line treated with polymeric NPs functionalized with folic acid. It is obvious that the efficiency of the treatment can be modulated by changing the concentration of the theranostic agent or the energy transmitted by irradiation to obtain the destruction of cancer cells.

5.3 Phototherapeutic effects: Translation to murine models

Lastly, the dual therapeutic performance of our HSA&phthaloNO$_2$-AB NPs was investigated *in vivo*, upon peri- and intra-tumoural tissue administration. Real-time *in vivo* thermal images (**Figure 5.7**) showed a 3.9 ˚C increase in temperature for mice treated with HSA&phthaloNO$_2$-AB NPs during 10 min exposure to a 660 nm LED lamp (0.05 W cm^{-2}).

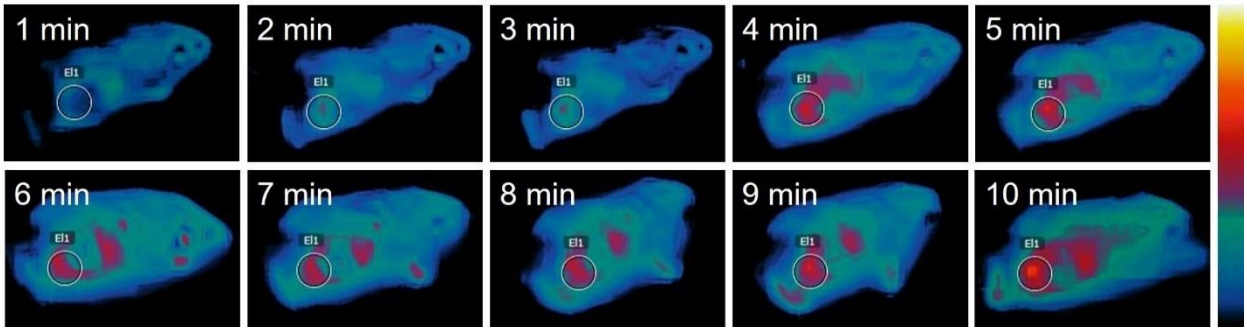

Figure 5.7. Thermal images of NIH:OVCAR3 tumour-bearing mouse, 4 h after peri- and intra-tumoural injection with HSA&phthaloNO$_2$-AB NPs, and exposed to 660 nm LED lamp for 10 min (0.05 W cm^{-2}); the white circle marks a narrow area of the tumour for which the average temperature was recorded.

The *ex vivo* histopathological assay (**Figure 5.8**) reported, by contrast with the control group, more prominent cellular atypia, frequent apoptotic images and larger areas of necrosis. It is unquestionable that our tailored HSA NPs loaded with deep red therapeutic and fluorescent molecules, and functionalized with specific cancer ligands, namely AB, are an effective approach for the therapy of cancer.

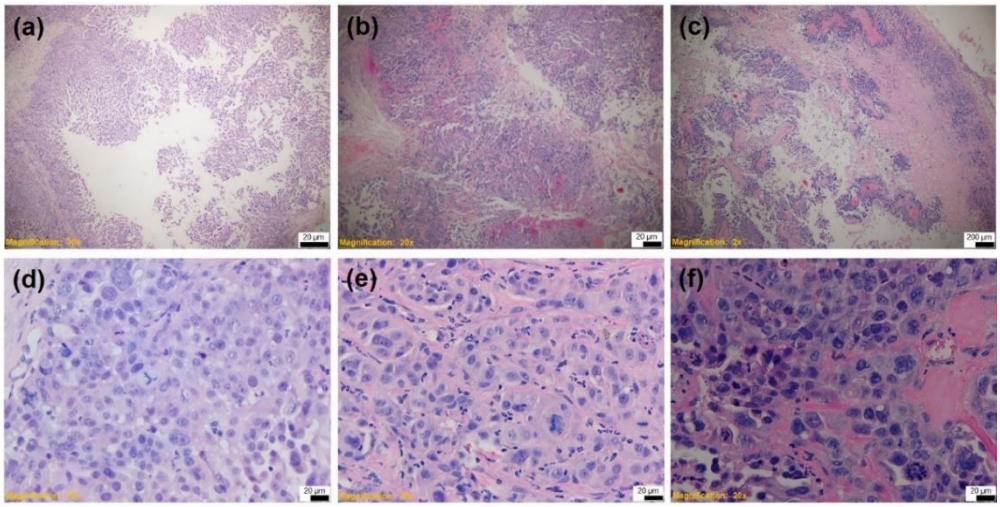

Figure 5.8. Hematoxylin and eosin (H&E) staining of excised tumours 24 hours after therapy: (a) and (d) control group, (b) and (e) HSA&phthaloNO$_2$-AB NPs administration, but without irradiation, (c) and (f) HSA&phthaloNO$_2$-AB NPs administration and irradiation; magnification x40 (a) to (c) and x400 (d) to (f).

All in vitro and in vivo studies were performed in collaboration with the Department of Radiobiology and Tumor Biology and the Department of Functional Genomics, Proteomics and Experimental Pathology, from the Oncology Institute "Prof. Dr. Ion Chiricuta", Cluj-Napoca, Romania and Department of Infectious Diseases, University of Agricultural Sciences and Veterinary Medicine, Cluj-Napoca, Romania.

Research results presented in this chapter have been published in Biomaterials Science, 9 (July 2021): 6183-6202 and Molecules 26(15) (August 2021): 4679, Journals.

Chapter 6. Revealing the potential of fluorophore-loaded protein-based nanoparticles for the interventional real-time imaging of ovarian cancer

6.1 Visible fluorescence imaging: FITC-loaded albumin nanoparticles

As **figure 6.1** depicts, after treatment with HSA&FITC-FA NPs an increase in fluorescent signal can be observed in the perinuclear region of NIH:OVCAR3 cells, possibly in the endoplasmic reticulum, as to the free FITC and untargeted HSA&FITC NPs treatments. The undesired nuclear internalization of free FITC, owing to the small size of the free molecule (smaller than the average nuclear pore of human cells, about 5 nm), can be easily observed in **figure 6.1** while no fluorescent signal coming from FITC fluorophores inside the nucleus is noted when cells were treated with HSA&FITC-FA NPs and HSA&FITC NPs.

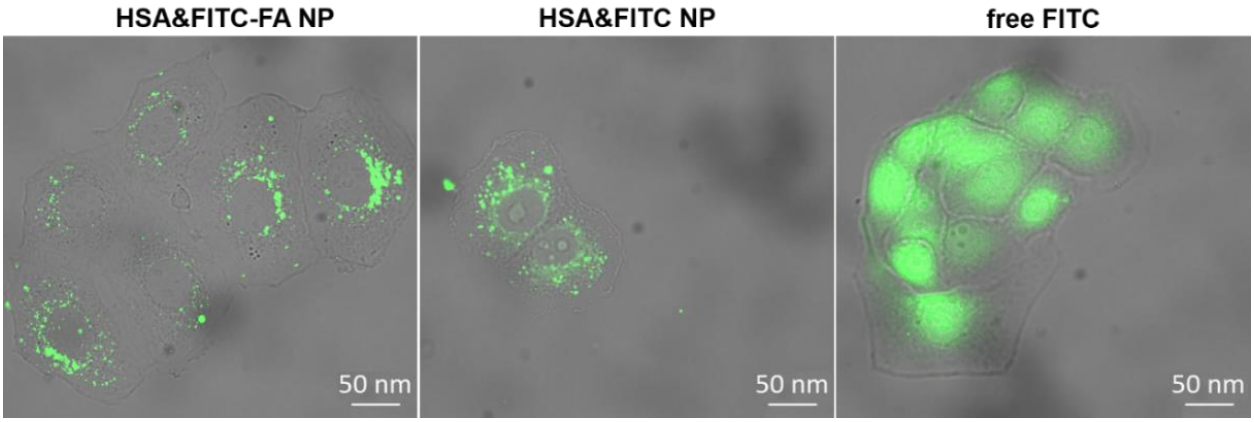

Figure 6.1. Fluorescence Microscopy Imaging of the NIH:OVCAR3 cells 6 h after treatment with HSA&FITC-FA NPs, HSA&FITC NPs and free FITC solution.

6.2 Deep red fluorescence imaging: phthaloNO$_2$-loaded albumin nanoparticles

To study the cellular internalization of the free phthaloNO$_2$ by ovarian cancer cells fluorescence microscopy was employed to capture cellular images of A2780 cells after 24 h incubation with the phototheranostic agent solution. As delineated in **figure 6.2**, the

fluorescence signal of the fluorophore is evenly distributed in the cytoplasm, while no nuclear internalization is observed. The control group presents no fluorescent signal.

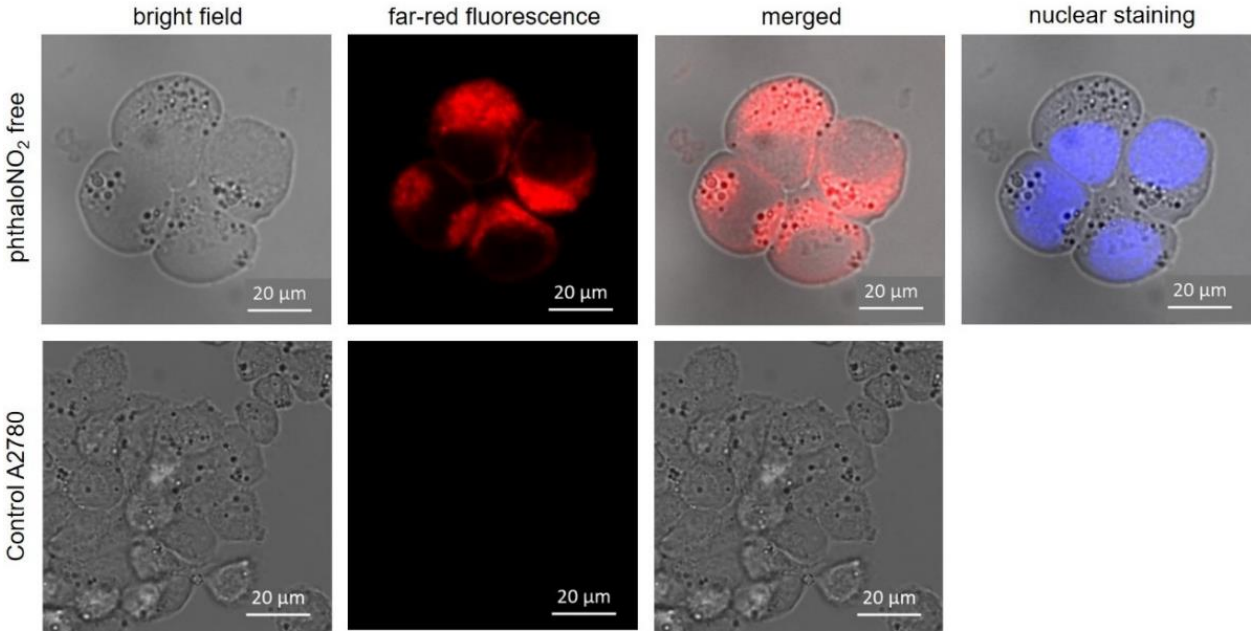

Figure 6.2. Fluorescence images of A2780 cells treated for 24h with phthaloNO$_2$ solution (top) and a control group without any treatment (bottom). The cells treated with phthaloNO$_2$ solution were stained with 4,6-diamidino-2-phenylindole (DAPI).

Next, for a better understanding of the HSA&phthaloNO$_2$-AB NPs targeting capability, *in vitro* fluorescence imaging was used to directly monitor the cellular uptake of HSA&phthaloNO$_2$-AB NPs in comparison with untargeted HSA&phthaloNO$_2$ NPs by A2780 cell line, known for the cell surface FRα expression, and A2780 Cis cell line, as negative control. When observing the A2780 cells, a better internalization is noticed for the HSA&phthaloNO$_2$-AB NPs at both 1 and 4 h incubation periods, compared to the non-specific cellular uptake of HSA&phthaloNO$_2$ NPs. In contrast, the fluorescence signal captured for the A2780 Cis line after treatment with the HSA&phthaloNO$_2$-AB NPs can be correlated to the cells treated with the undecorated HSA&phthaloNO$_2$ NPs at both time intervals (**Figure 6.3**). These results uphold the AB decorated HSA&phthaloNO$_2$ NPs active targeting capacity of the FRα protein frequently overexpressed on ovarian cancer cells. In all cases, no nuclear internalization of the HSA&phthaloNO$_2$ NPs or HSA&phthaloNO$_2$-AB NPs was observed.

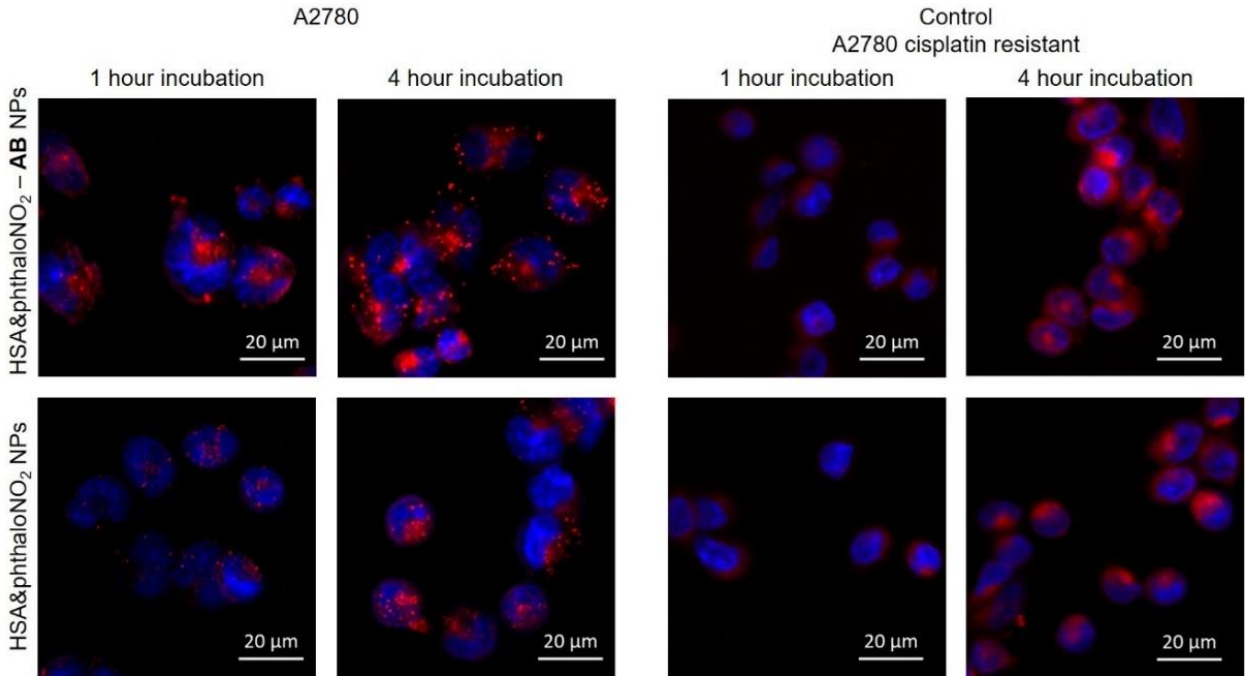

Figure 6.3. Fluorescence images of A2780 (left) and control A2780 Cis (right) cells after 1 and 4 h of treatment with HSA&phthaloNO$_2$-AB NPs (top) and HSA&phthaloNO$_2$ NPs (bottom). The cells were stained with DAPI.

FLIM analysis

Furthermore, by bringing together time- and spatially resolved fluorescence measurements, FLIM technique is able to detect local interactions of fluorescent phthaloNO$_2$ molecules, including their different states upon encapsulation within HSA NPs and intracellular localization. Thus, *in vitro* FLIM was implemented as a decoding approach to determine the fluorescence lifetime as function of the localization of HSA&phthaloNO$_2$-AB NPs, HSA&phthaloNO$_2$ NPs and free phthaloNO$_2$ within A2780 cancer cells (**Figure 6.4**).

Next, A2780 ovarian cancer cells were treated and incubated for 4 h with the HSA&phthaloNO$_2$-AB NPs, HSA&phthaloNO$_2$ NPs and free phthaloNO$_2$, and the lifetime profiles and histograms of the phototheranostic agent were recorded (**Figure 6.5, table 6.1**); control A2780 cells without treatment were imaged as well. The fluorescence lifetime decay curves extracted from the spot marked with red in **figure 6.4** namely the cytosol of cells, reveal an 0.18 ns increase in the $\tau_{AV\,int}$ of phthaloNO$_2$ once encapsulated within the HSA NPs (**Figure 6.5)**, suggesting that the phototheranostic molecules are bound within the HSA protein. Moreover, the 0.23 ns increase in the $T_{AV\,int}$ of the HSA&phthaloNO$_2$-AB NPs compared to the not AB decorated HSA&phthaloNO$_2$ NPs can be attributed to the different localization of the phototheranostic agent within the cell [10] once the internalization pathway of the HSA&phthaloNO$_2$-AB NPs is mediated by FRα. Thus, by

monitoring the lifetime of AB decorated fluorescent NPs within biological systems, cells that overexpress FRα at the surface of their membrane can be distinguish in a simpler and neater way. The control cells showed negligible auto-fluorescence.

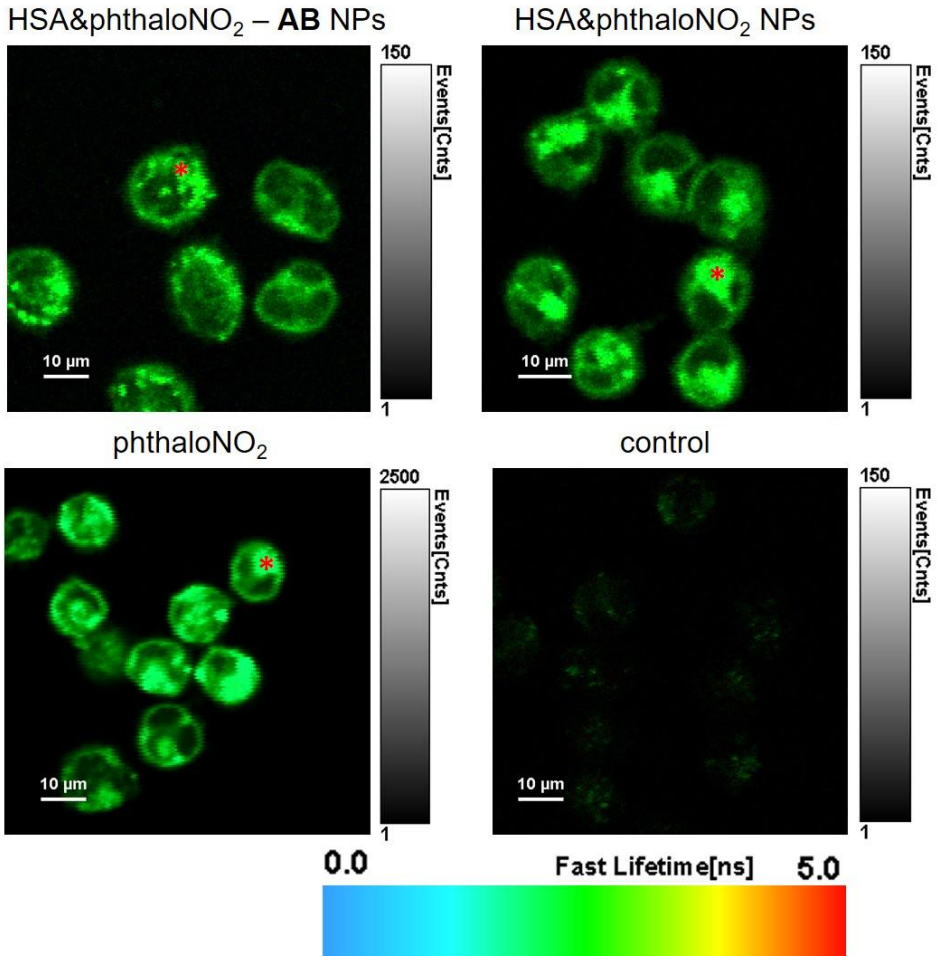

Figure 6.4. FLIM images of A2780 after 4 h of treatment with HSA&phthaloNO$_2$-AB NPs, HSA&phthaloNO$_2$ NPs, phthaloNO$_2$ and control cells without treatment. The red mark indicates the spot from where the fluorescence lifetime decay curves were extracted.

Table 6.1. Lifetime decays and population percentages for HSA&phthaloNO$_2$-AB NPs, HSA&phthaloNO$_2$ NPs and phthaloNO$_2$ after internalization into A2780 cells (4 h incubation period).

	$\tau_{AV\ int}$ (ns)	A_1 (%)	τ_1 (ns)	A_2 (%)	τ_2 (ns)	χ^2
HSA&phthaloNO$_2$-AB NPs	2.31 ± 0.01	59	2.66 ± 0.04	41	1.16 ± 0.03	1.04
HSA&phthaloNO$_2$ NPs	2.08 ± 0.01	57	2.41 ± 0.01	43	1.01 ± 0.01	1.01
phthaloNO$_2$	1.90 ± 0.01	53	2.25 ± 0.02	47	1.10 ± 0.01	1.21

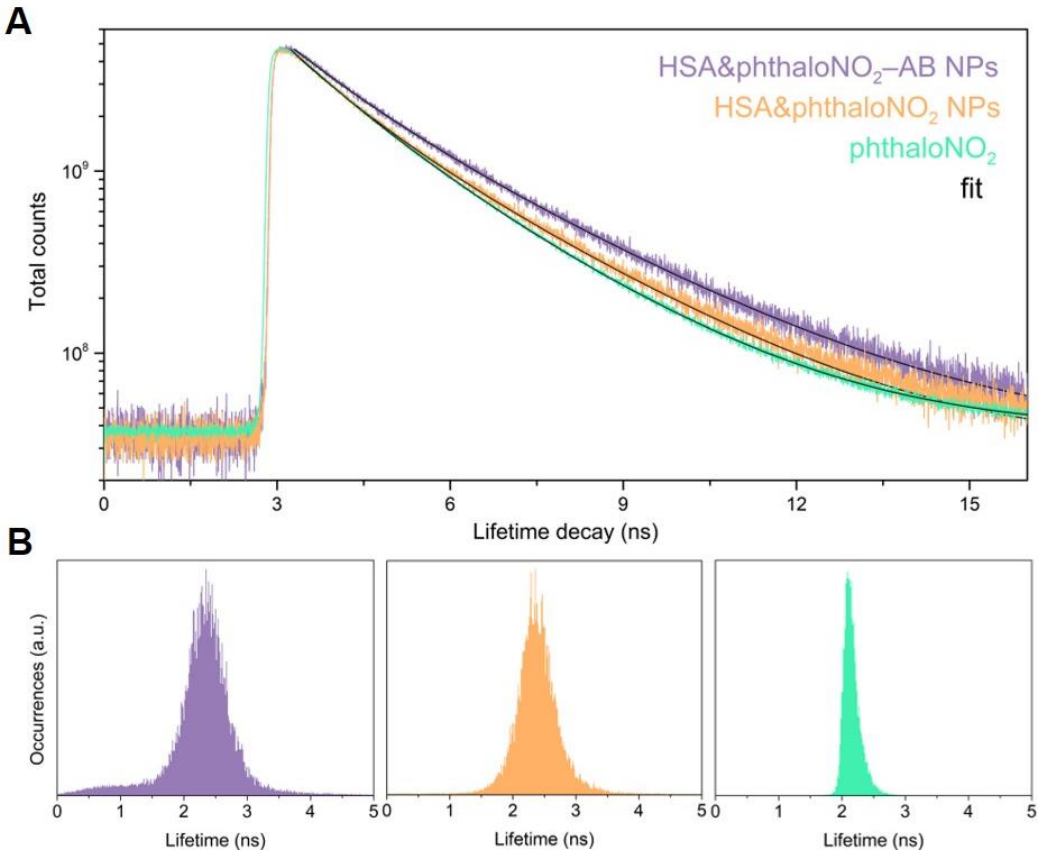

Figure 6.5. (A) Lifetime decay curves extracted from the spot marked with red in **figure 6.4** and (B) histograms recorded for the phototheranostic agent in the cytoplasm of A2780 cells 4 h after treatment with HSA&phthaloNO$_2$-AB NPs (violet), HSA&phthaloNO$_2$ NPs (yellow), and phthaloNO$_2$ solution (green).

6.3 NIR fluorescence imaging: ICG-loaded albumin nanoparticles

In order to prove the internalization of HSA&ICG NPs in the same pattern, NIR fluorescence microscopy images of NIH:OVCAR3 ovarian cancer cells treated for 24 h with free ICG and ICG-loaded HSA NPs were collected and presented in **figure 6.6**. Both the HSA&ICG NPs and ICG treated cells present no nuclear internalization, while a more evenly dispersion within the cytoplasm can be observed for the free fluorophore. Moreover, for the HSA&ICG NPs treated cells the apparition of highly fluorescent vesicles (probably caveosomes) can be distinguished.

Hence, this incipient fluorescence imaging studies presented in this chapter are just the stepping stone of a broader research project (project number PN-III-P4-ID-PCCF-2016-0142, within PNCDI III). The aim of the project is focused on the development of targeted NIR fluorophore-loaded NPs and attesting them as contrast agents for the NIR fluorescence-guided cancer surgery, by NIR *in vivo* and *ex vivo* imaging investigation of

murine models and tissues removed from cancer patients after administration or treatment with NIR fluorophore-loaded NPs.

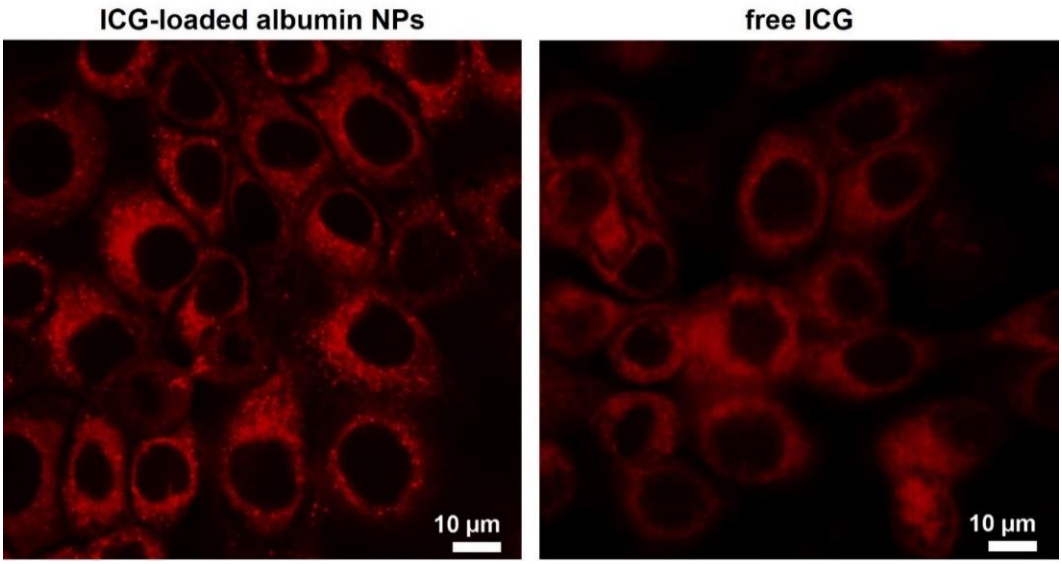

Figure 6.6. Fluorescence Microscopy Imaging of NIH:OVCAR3 cells treated with HSA&ICG NPs vs. free ICG.

To conclude, thanks to their enlarged size, surface chemistry and ability to bind with cancer-specific ligands for an active targeting, protein-based NPs loaded with various NIR fluorophores promise prolonged blood circulation time and enhanced accumulation in the tumour site. The feasibility and biocompatibility of NIR fluorescent protein-based NPs as contrast agents for the real-time interventional NIR fluorescence imaging of cancer has been previously testified by a notable number of preclinical animal studies. Overall, it may be said that NIR fluorophore loaded protein-based NPs have the potential to be translated in the near future as contrast agents for the real-time NIR fluorescence image guided surgery of cancer.

All in vitro studies were performed in collaboration with the Department of Radiobiology and Tumor Biology from the Oncology Institute "Prof. Dr. Ion Chiricuta", Cluj-Napoca, Romania

Research results presented in this chapter have been published in Nanotechnology, 31, no. 31 (July 2020): 315102 and Biomaterials Science, 9 (July 2021): 6183-6202, Journals

Final conclusions and perspectives

"Science is not only a disciple of reason but also one of romance and passion."

Stephen Hawking

In pursuance of better post-operative outcomes and considerable improvements in the quality of life of cancer patients, there is a great need for a new generation of approaches and nanotools able to cure cancer. Ergo, my doctoral thesis aims to design up-to-the-minute new nano-sized phototheranostic agents with potential to surpass the limitations of the classical methods used nowadays in cancer detection and surgical planning. Thus, we design novel phototheranostic agents with optical features in the biological window of the electromagnetic spectrum, by encapsulating two FDA-approved fluorophores and two newly synthesized phthalocyanine dyes within biocompatible albumin NPs for the targeted fluorescence imaging and synergistic dual therapy of ovarian cancer.

First, albumin NPs, precisely HSA and BSA, loaded with two different FDA approved dyes, FITC and ICG, and two phthalocyanine dyes, phthaloNO_2 and phthaloNH_2, are successfully fabricated following a two-step procedure: desolvation using ethanol and stabilization by chemical cross-linking with Gal.

- The high reproducibility of the synthesis, and great particle yield, over 75%, was proven for all four classes of fluorophore-loaded albumin NPs.
- The spectroscopic characterization of the afresh designed albumin NPs reveals excellent fluorescence conservation for all four dyes after encapsulation within the albumin NPs.
- The monodispersity and average diameter, of 27 nm, of the fluorophore-loaded albumin NPs are investigated and proved via TEM imaging and DLS measurements; their negative charged surface (-12 to -15 mV) was revealed by zeta-potential investigations.

Afterward, for the specific targeting of the FRα overexpressed at the surface of nearly all ovarian cancer cell lines, i.e., NIH:OVCAR3 and A2780 cell lines herein selected for *in vitro* studies, the newly synthesized fluorophore-loaded albumin based NPs are further decorated by covalent conjugation with FA and AB.

- By employing DLS and zeta-potential investigations the successful biofunctionalization of the albumin NPs with the two ovarian cancer-targeting ligands is confirmed.
- The great size stability of the albumin NPs, 7 days after the synthesis, is confirmed by DLS measurements.
- The HSA&FITC and HSA&ICG NPs present excellent fluorescence stability in time and is maintained 15 days after synthesis: 92 and 111%, respectively, of their initial fluorescence intensity is.

Next, three ovarian cancer cell lines, namely NIH:OVCAR3, A2780 and A2780 Cis, are employed to test and confirm the good biocompatibility of all fluorophores and fluorophore-loaded albumin NPs. The improved targeting capabilities of the bioconjugated fluorophore-loaded albumin NPs *in vitro* are tested by fluorescence and TEM imaging.

- The viability of ovarian cancer cells treated with the newly synthesized albumin NPs is confirmed via MTT assay.
- Cellular uptake efficiency through FRα-mediated endocytosis in ovarian cancer cells is highly increased after bioconjugation of the albumin NPs with specific cancer-targeting molecules, as observed by TEM imaging.

The efficiency of the afresh fluorophore-loaded albumin NPs as dual therapeutic agents in biomedical applications is thoroughly investigated. Their photodynamic and photothermal effects are firstly evaluated in solution and thanks to their promising therapeutic capabilities, various *in vitro* studies are further conducted on A2780 cells.

- The great $^{1}O_2$ quantum yield, 43%, of the HSA&phthaloNO$_2$ NPs, good light-to-heat conversion efficiency, 8.5%, and excellent photostability of the HSA&phthaloNH$_2$ NPs are calculated and studied in solution, by exposure to a 660 nm LED lamp.
- Their cytotoxic effect due to the light-to-heat conversion and ROS generation is confirmed *in vitro* by employing fluorescence imaging, MTT and flowcytometry investigations.
- Flowcytometry assay revealed 97% of the cancer cells treated with HSA&phthaloNO$_2$ NPs die after exposure to irradiation with a 660 nm LED lamp.

In addition, the translation of our research to murine models allows us to study the *in vivo* viability and phototherapeutic features of the newly synthesized HSA&phthaloNO$_2$-AB NPs. The functionalized fluorophore-loaded albumin NPs are successfully administrated to ovarian cancer tumour bearing mice by peri- and intra-tumoural tissue injection, 4 h prior to irradiation with a 660 nm LED lamp (0.05 W cm^{-2}). NIH:OVCAR3 ovarian cancer cell line was selected for these experiments.

- The surface temperature change of mice is monitored with ease in real-time during the 10 min exposure to the LED lamp.
- A maximum increase in temperature of 3.9 ˚C is recorded in the tumour site for mice injected with HSA&phthaloNO$_2$-AB NPs, while no change in temperature is observed for the control group.
- Histopathological assay reports frequent apoptotic images, larger areas of necrosis and more prominent cellular atypia for the HSA&phthaloNO$_2$-AB NPs-treated and exposed to light group, by contrast to the control group, without irradiation.

The fluorescence properties and successful bioconjugation with FA and AB of the HSA&FITC and HSA&phthaloNO$_2$ NPs are carefully investigated in solution, as well as *in vitro,* after internalization within the ovarian cancer cell lines NIH:OVCAR3 and A2780.

- The increased internalization of the AB-conjugated albumin NPs is confirmed by fluorescence imaging; A2780 Cis cell line is studied as negative control of the FRα overexpression.
- FLIM investigations highlight the difference in fluorescence lifetime of AB decorated (2.31 ns) and non-decorated albumin NPs (2.08 ns), probably due to a different internalization pathway for the groups of fluorophore-loaded albumin NPs, thus also confirming the FRα mediated internalization pathway for AB-decorated albumin NPs.
- By studying the fluorescence lifetime of our HSA&phthaloNO$_2$-AB NPs in biological systems, a new insight to discern cancer cells that overexpress FRα at their surface comes to life.

Thus, by embracing the nanotechnological advancements in the field of medical science, researchers working in the area of cancer therapy and imaging are looking for the next breakthrough treatment strategy to ensure lower cancer recurrence rates and improved outcomes for patients. Herein, to outdo the side effects, low photostability and non-specific targeting of standard free dye administration, albumin-based NPs are developed to aptly encapsulate and target the four different fluorescent molecules to the desired type of cancer cells, namely ovarian cancer cells. The nano-sized agents display great biocompatibility, enhanced aqueous biostability and photothermal activity as well as high ROS generation efficiency. To achieve active targeting of the desired malignant tissue and suppress the rapid clearance of the photosensitive agents from the peritoneal cavity, the NPs are biofunctionalized with ovarian cancer-appropriate ligands. In comparison with most theranostic nanoplatforms developed until today, our proof-of-concept phototheranostic NPs reveal great photothermal, photodynamic and fluorescence imaging features simultaneously. Thus, in conclusion:

- *We have successfully fabricated four classes of biocompatible fluorophore-loaded albumin NPs that exhibit both high loading efficiency (ranging from 91% for*

phthaloNH$_2$, 88% for phthaloNO$_2$, 50% for ICG, and over 30% for FITC) and sustainable fluorescence emission in solution and cancer cells.

- *We have clearly demonstrated the increased cellular uptake of the newly fabricated albumin NPs after their bioconjugation with specific targeting molecules against FRα overexpressed at the surface of ovarian cancer cells.*
- *We revealed and validated interesting phototheranostic properties of all four classes of fluorophore-loaded albumin NPs, especially for HSA&phthaloNO$_2$ NPs and HSA&phthaloNH$_2$ NPs, with real potential for dual PDT-PTT phototherapy.*
- *Our preliminary confocal NIR microscopy studies conducted on the newly installed re-scan confocal microscope confirm the feasibility of HSA&ICG NPs as potential NIR fluorescent contrast agents for the real-time image-guided surgery of cancer.*
- *All in all, the functionalized fluorophore-loaded albumin NPs present promising result as therapeutic and fluorescent agents for the targeted imaging and therapy of ovarian cancer.*

As perspectives, out of the two fluorophores with optical properties in the visible domain, albumin NPs loaded with phthaloNO$_2$ should be considered for further investigations, thanks to the dual phototherapeutic properties and imaging capabilities. Vis-à-vis the NIR emitting fluorophores, considering the novelty and improved performances after encapsulation within the protein NPs, phthaloNH$_2$ may be considered for pre-clinical, or even clinical studies, in the near future. Moreover, due to the encouraging results obtained after performing *in vivo* studies on murine models, further work directions should be carefully considered:

- *In vivo PTT evaluation and histopathological assay for mice treated with HSA&ICG and BSA&phthaloNH$_2$ NPs.*
- *Functionalization of the fluorophore-loaded albumin NPs with targeting molecules appropriate for other types of cancer.*
- *Co-functionalization of the fluorophore-loaded albumin NPs with various cancer-drugs, e.g., Abraxane, Cytoxan, Doxil, Taxol.*
- *In vivo fluorescence microscopy imaging in murine models after administration of all four afresh synthesized albumin NPs.*
- *Ex vivo imaging investigation of tissues removed from cancer patients after incubation with NIR fluorophore-loaded NPs.*

References

1. Copur, M. S. State of Cancer Research Around the Globe. *Oncology (Williston Park, N.Y.)* **33**, 181–185 (2019).
2. Roser, M. & Ritchie, H. Cancer. *Our World in Data* (2015).
3. Baydoun, M. *et al.* Photodynamic Therapy Using a New Folate Receptor-Targeted Photosensitizer on Peritoneal Ovarian Cancer Cells Induces the Release of Extracellular Vesicles with Immunoactivating Properties. *JCM* **9**, 1185 (2020).
4. Zhang, R. R. *et al.* Beyond the margins: real-time detection of cancer using targeted fluorophores. *Nat Rev Clin Oncol* **14**, 347–364 (2017).
5. van Driel, P. B. A. A. *et al.* Characterization and Evaluation of the Artemis Camera for Fluorescence-Guided Cancer Surgery. *Mol Imaging Biol* **17**, 413–423 (2015).
6. Haque, A., Faizi, Md. S. H., Rather, J. A. & Khan, M. S. Next generation NIR fluorophores for tumor imaging and fluorescence-guided surgery: A review. *Bioorganic & Medicinal Chemistry* **25**, 2017–2034 (2017).
7. Solomon, S. B. & Silverman, S. G. Imaging in Interventional Oncology. *Radiology* **257**, 624–640 (2010).
8. de Boer, E. *et al.* Optical innovations in surgery: Optical innovations in surgery. *Br J Surg* **102**, e56–e72 (2015).
9. Silindir-Gunay, M., Sarcan, E. T. & Ozer, A. Y. Near-infrared imaging of diseases: A nanocarrier approach. *Drug Dev Res* ddr.21532 (2019) doi:10.1002/ddr.21532.
10. Mroz, P., Yaroslavsky, A., Kharkwal, G. B. & Hamblin, M. R. Cell Death Pathways in Photodynamic Therapy of Cancer. *Cancers* **3**, 2516–2539 (2011).
11. Chen, C. *et al.* Calixarene-Based Supramolecular AIE Dots with Highly Inhibited Nonradiative Decay and Intersystem Crossing for Ultrasensitive Fluorescence Image-Guided Cancer Surgery. *Angew. Chem. Int. Ed.* **59**, 10008–10012 (2020).
12. Alves, C. G., Lima-Sousa, R., de Melo-Diogo, D., Louro, R. O. & Correia, I. J. IR780 based nanomaterials for cancer imaging and photothermal, photodynamic and combinatorial therapies. *International Journal of Pharmaceutics* **542**, 164–175 (2018).
13. Chen, H., Tian, J., He, W. & Guo, Z. H_2O_2-Activatable and O_2-Evolving Nanoparticles for Highly Efficient and Selective Photodynamic Therapy against Hypoxic Tumor Cells. *J. Am. Chem. Soc.* **137**, 1539–1547 (2015).
14. Sandra, F., Khaliq, N. U., Sunna, A. & Care, A. Developing Protein-Based Nanoparticles as Versatile Delivery Systems for Cancer Therapy and Imaging. *Nanomaterials (Basel)* **9**, (2019).
15. Pan, G.-Y. *et al.* Dual Channel Activatable Cyanine Dye for Mitochondrial Imaging and Mitochondria-Targeted Cancer Theranostics. *ACS Biomater. Sci. Eng.* **3**, 3596–3606 (2017).
16. Donohoe, C., Senge, M. O., Arnaut, L. G. & Gomes-da-Silva, L. C. Cell death in photodynamic therapy: From oxidative stress to anti-tumor immunity. *Biochimica et Biophysica Acta (BBA) - Reviews on Cancer* **1872**, 188308 (2019).
17. Campu, A. *et al.* ICG-loaded gold nano-bipyramids with NIR activatable dual PTT-PDT therapeutic potential in melanoma cells. *Colloids and Surfaces B: Biointerfaces* **194**, 111213 (2020).
18. Gao, Q. *et al.* Gold Nanoparticles in Cancer Theranostics. *Front. Bioeng. Biotechnol.* **9**, 647905 (2021).
19. *Advances in Nanotheranostics I*. vol. 6 (Springer Berlin Heidelberg, 2016).
20. Pansare, V. J., Hejazi, S., Faenza, W. J. & Prud'homme, R. K. Review of Long-Wavelength Optical and NIR Imaging Materials: Contrast Agents, Fluorophores, and Multifunctional Nano Carriers. *Chem. Mater.* **24**, 812–827 (2012).

21. Yu, J. *et al.* Near-infrared fluorescence imaging using organic dye nanoparticles. *Biomaterials* **35**, 3356–3364 (2014).
22. Chu, L. *et al.* Biocompatible near-infrared fluorescent nanoparticles for macro and microscopic in vivo functional bioimaging. *Biomed. Opt. Express* **5**, 4076 (2014).
23. Madamsetty, V. S., Mukherjee, A. & Mukherjee, S. Recent Trends of the Bio-Inspired Nanoparticles in Cancer Theranostics. *Front. Pharmacol.* **10**, 1264 (2019).
24. Tarhini, M., Greige-Gerges, H. & Elaissari, A. Protein-based nanoparticles: From preparation to encapsulation of active molecules. *Int J Pharm* **522**, 172–197 (2017).
25. Wang, E. C. & Wang, A. Z. Nanoparticles and their applications in cell and molecular biology. *Integrative Biology* **6**, 9–26 (2014).
26. Gou, Y. *et al.* Bio-Inspired Protein-Based Nanoformulations for Cancer Theranostics. *Front. Pharmacol.* **9**, 421 (2018).
27. Chen, Q., Liang, C., Wang, C. & Liu, Z. An Imagable and Photothermal “Abraxane-Like” Nanodrug for Combination Cancer Therapy to Treat Subcutaneous and Metastatic Breast Tumors. *Adv. Mater.* **27**, 903–910 (2015).
28. Sheng, Z. *et al.* Smart Human Serum Albumin-Indocyanine Green Nanoparticles Generated by Programmed Assembly for Dual-Modal Imaging-Guided Cancer Synergistic Phototherapy. *ACS Nano* **8**, 12310–12322 (2014).
29. Hu, Z., Chen, W.-H., Tian, J. & Cheng, Z. NIRF Nanoprobes for Cancer Molecular Imaging: Approaching Clinic. *Trends in Molecular Medicine* **26**, 469–482 (2020).
30. Egloff-Juras, C., Bezdetnaya, L., Dolivet, G. & Lassalle, H.-P. NIR fluorescence-guided tumor surgery: new strategies for the use of indocyanine green. *IJN* **Volume 14**, 7823–7838 (2019).
31. Borlan, R. *et al.* Design of fluorophore-loaded human serum albumin nanoparticles for specific targeting of NIH:OVCAR3 ovarian cancer cells. *Nanotechnology* **31**, 315102 (2020).
32. Cohen, S. & Margel, S. Engineering of near IR fluorescent albumin nanoparticles for in vivo detection of colon cancer. *J Nanobiotechnol* **10**, 36 (2012).
33. Weber, C., Coester, C., Kreuter, J. & Langer, K. Desolvation process and surface characterisation of protein nanoparticles. *International Journal of Pharmaceutics* **194**, 91–102 (2000).
34. Wong, R. C. H., Lo, P.-C. & Ng, D. K. P. Stimuli responsive phthalocyanine-based fluorescent probes and photosensitizers. *Coordination Chemistry Reviews* **379**, 30–46 (2019).
35. Li, X. *et al.* Phthalocyanines as medicinal photosensitizers: Developments in the last five years. *Coordination Chemistry Reviews* **379**, 147–160 (2019).
36. Zheng, B.-D., He, Q.-X., Li, X., Yoon, J. & Huang, J.-D. Phthalocyanines as contrast agents for photothermal therapy. *Coordination Chemistry Reviews* **426**, 213548 (2021).
37. Ishii, K. Functional singlet oxygen generators based on phthalocyanines. *Coordination Chemistry Reviews* **256**, 1556–1568 (2012).
38. Molecular weight and isoelectric point of various immunoglobulins. https://www.agrisera.com/en/info/molecular-weight-and-isoelectric-point-of-various-immunoglobulins.html.
39. Champeau, M., Vignoud, S., Mortier, L. & Mordon, S. Photodynamic therapy for skin cancer: How to enhance drug penetration? *Journal of Photochemistry and Photobiology B: Biology* **197**, 111544 (2019).
40. Ruhi, M. K., Ak, A. & Gülsoy, M. Dose-dependent photochemical/photothermal toxicity of indocyanine green-based therapy on three different cancer cell lines. *Photodiagnosis and Photodynamic Therapy* **21**, 334–343 (2018).
41. Doshi, M. *et al.* Conducting polymer nanoparticles for targeted cancer therapy. *RSC Adv.* **5**, 37943–37956 (2015).

Dissemination

Papers

Thesis-related publications

'Fluorescent Phthalocyanine-Encapsulated Bovine Serum Albumin Nanoparticles: Their Deployment as Therapeutic Agents in the NIR Region'

Raluca Borlan, Daria Stoia, Luiza Gaina, Andreea Campu, Gabriel Marc, Maria Perde-Schrepler, Mihaela Silion, Dana Maniu, Monica Focsan and Simion Astilean
Molecules, 26(15) (**August 2021**): 4679, IF: 4.411 and AIS: 0.694
DOI: 10.3390/molecules26154679

'Antibody Functionalized Theranostic Protein Nanoparticles for Synergistic Deep Red Fluorescence Imaging and Multimodal Therapy of Ovarian Cancer'

Raluca Borlan, Monica Focsan, Maria Perde-Schrepler, Olga Soritau, Andreea Campu, Luiza Gaina, Emoke Pall, Bogdan Pop, Oana Baldasici, Claudia Gherman, Daria Stoia, Dana Maniu and Simion Astilean
Biomaterials Science, 9 (**July 2021**): 6183-6202, IF: 6.843 and AIS: 1.102
DOI: 10.1039/D1BM01002F

'Interventional NIR Fluorescence Imaging of Cancer: Review on Next Generation of Dye-Loaded Protein-Based Nanoparticles for Real-Time Feedback During Cancer Surgery'

Raluca Borlan, Monica Focsan, Dana Maniu, and Simion Astilean
International Journal of Nanomedicine, 16 (**March 2021**): 2147–71, IF: 6.400 and AIS: 0.953
DOI: 10.2147/IJN.S295234

'Design of Fluorophore-Loaded Human Serum Albumin Nanoparticles for Specific Targeting of NIH:OVCAR3 Ovarian Cancer Cells'

Raluca Borlan, Andra-Sorina Tatar, Olga Soritau, Dana Maniu, Gabriel Marc, Adrian Florea, Monica Focsan, and Simion Astilean
Nanotechnology, 31(31) (**July 2020**): 315102, IF: 3.874 and AIS: 0.680
DOI: 10.1088/1361-6528/ab8b90

'NIR Fluorescence Captures Clear Images of Cancerous Tumors During Surgery'

Raluca Borlan, Monica Focsan, Patriciu Achimas-Cadariu and Simion Astilean
Biophotonics magazine, **September 2021**

Co-authored publications

'Folic Acid Functionalized Gold Nanoclusters for Enabling Targeted Fluorescence Imaging of Human Ovarian Cancer Cells'

Hada, Alexandru-Milentie, Ana-Maria Craciun, Monica Focsan, Raluca Borlan, Olga Soritau, Milica Todea, and Simion Astilean
Talanta, 225 (**April 2021**): 121960, IF: 6.057 and AIS: 0.830
DOI: 10.1016/j.talanta.2020.121960

'ICG-Loaded Gold Nano-Bipyramids with NIR Activatable Dual PTT-PDT Therapeutic Potential in Melanoma Cells'

Andreea Campu, Monica Focsan, Frederic Lerouge, Raluca Borlan, Leopold Tie, Dumitrita Rugina, and Simion Astilean
Colloids and Surfaces B: Biointerfaces, 194 (**October 2020**): 111213, IF: 5.268 and AIS: 0.711
DOI: 10.1016/j.colsurfb.2020.111213

Conference participations

Oral presentations

*'*Design of protein-based nanoparticles loaded with FDA approved fluorophores for specific targeting of ovarian cancer cells'

Raluca Borlan, Andra-Sorina Tatar, Olga Soritau, Dana Maniu, Monica Focsan, and Simion Astilean
Conferinței Naționale a Doctoranzilor de la Facultățile de Fizică din cadrul Universităților din Consorțiul Universitaria, **October 2020**, Iasi, Romania

*'*Sinteza și caracterizarea spectroscopică a unor nanoparticule proteice încărcate cu verde de indocianină pentru aplicații biomedicale'

Raluca Borlan, Andra-Sorina Tatar, Olga Soritau, Dana Maniu, Monica Focsan, and Simion Astilean
Conferinței Naționale a Doctoranzilor de la Facultățile de Fizică din cadrul Universităților din Consorțiul Universitaria, **December 2019**, Bucharest, Romania

Poster presentations

'Resveratrol-therapeutic agent delivered and localized via fluorescent polyelectrolyte microsystems inside living cells'

Daria Stoia, Roxana Popan, Madalina Nistor, Raluca Borlan, Dumitrita Rugina and Monica Focsan
18th International Conference on Nanoscience & Nanotechnologies, **July 2021**, Thessaloniki, Greece

'Indocyanine green–loaded protein nanoparticles for near infrared imaging and targeting of ovarian cancer cells'

Raluca Borlan, Andra-Sorina Tatar, Dana Maniu, Olga Soritau, Eva Fischer, Monica Focsan, Achimas-Cadariu Patriciu and Simion Astilean
18th European Conference on Spectroscopy of Biological Molecules, **August 2019**, Dublin, Ireland

Participation in research projects

- New Targeted Optical Imaging Nanoprobes for Near-Infrared (NIR) Real-Time (RT) Image-Guided Surgery of Ovarian Cancer, Project director: Prof. Dr. Simion Astilean, UEFISCDI Project number: PN-III-P4-ID-PCCF-2016-0142 (member)

- Emerging Molecular Technologies Based on Micro and Nano-Structured Systems with Biomedical Applications, Leader UBB: Prof. Dr. Simion Astilean, UEFISCDI Project number: PN-III-P1-1.2-PCCDI2017-0010 (member)

- Theranostic Microplatforms for Multimodal Therapy in Human Eye Diseases, A New Paradigm for The Biomedical Applications, Leader UBB: CS I. Dr. Monica Focsan, UEFISCDI Project number: PN-III-P2-2.1-PED-2019-4558 (member)

This thesis was financially supported by the research project NEW TARGETED OPTICAL IMAGING NANOPROBES FOR NEAR-INFRARED (NIR) REAL-TIME (RT) IMAGE-GUIDED SURGERY OF OVARIAN CANCER (PN-III-P4-ID-PCCF-2016-0142), within PNCDI III (project director Prof. Dr. Simion Astilean) and by the Research Funds for Doctoral Grants from the Babes-Bolyai University, Cluj-Napoca, Romania.